

DESIGN, FABRICATION AND CHARACTERIZATION OF A RF MEMS BASED RECONFIGURABLE ANTENNA

by
REY ALBERTO FEBO

A proposal submitted in partial fulfillment of the requirements for the degree of

MASTER OF SCIENCE
in
ELECTRICAL ENGINEERING

UNIVERSITY OF PUERTO RICO
MAYAGÜEZ CAMPUS
2009

Approved by:

Nivia Colón Díaz, MS
Member, Graduate Committee

Date

Rafael A. Rodríguez Solís, PhD
Member, Graduate Committee

Date

José Colom Ustariz, PhD
Member, Graduate Committee

Date

Nelson Sepúlveda Alancastro, PhD
President, Graduate Committee

Date

Edgar Acuña, PhD
Representative of Graduate Studies

Date

Ramón Vázquez Espinosa, PhD
Dean of Engineering and Acting Chairman of ECE Dept.

Date

ABSTRACT

DESIGN, FABRICATION AND CHARACTERIZATION OF A RF MEMS BASED RECONFIGURABLE ANTENNA

By

Rey Alberto Febo

In order to satisfy an increasing need to operate in network systems with different standards and operating frequencies, new ideas for next generation communication systems are needed. The sudden increase of this need has forced the creation of tunable and reconfigurable devices all around the electronics and electromagnetic fields. RF MEMS arrived to the design table since they have proven to be more functional, lighter, and more reliable than their solid state counterparts for low and medium power handling applications. It's a way to provide the scientific community with a more efficient way of using the available bandwidth and to achieve a higher data transmission rate for an increasing amount of users.

MEMS deal with the integration of mechanical elements, actuators, electronics and sensors on a common substrate through a process of microfabrication. They are fabricated using compatible micromachining processes, selectively etching away or adding new structural layers to develop an electromechanical systems. The implementation of these devices has improved some applications in the antennas field and has created innovative ways of changing the current RF systems.

In this thesis, the design, fabrication process, and characterization of an RF MEMS-based reconfigurable antenna is presented. The fabrication process took place in the packaging laboratory at the Air Force Research Laboratory at Wright Patterson Air Force Base, Ohio. The antenna design was simulated in CST Microwave Studio. The biasing lines will be designed to have the least effect on the antenna performance. A probe feeding technique will be employed. The integration of the RF MEMS switches was done via wire bonding. The main goal is to achieve antenna frequency tuning capability by changing the geometry of the antenna using RF MEMS switches. The radiation pattern of the antenna will also be observed for characterization purposes.

RESUMEN

Para satisfacer la necesidad de operar en sistemas con diferentes estándares y frecuencias de operación se necesitan nuevas ideas para la nueva generación de sistemas de comunicación. El incremento repentino de dicha necesidad ha forzado la creación de dispositivos reconfigurables o de multiusos alrededor de los campos de electrónica y electromagnética. Los RF MEMS llegan a la mesa de diseño ya que han demostrado que proveen mayor funcionalidad, son más livianos y más confiables que sus contrapartes de estado sólido para aplicaciones que requieren linealidad y bajo consumo de potencia. Es una forma de proveer a la comunidad científica con una manera más eficiente de usar el ancho de banda disponible y para adquirir una transmisión de data mayor para un número de usuarios que sigue incrementando.

MEMS se refiere a la integración de elementos mecánicos, actuadores, electrónica y sensores en un sustrato común por medio de un proceso de microfabricación. Ellos son fabricados usando procesos de microfabricación compatibles, descartando selectivamente el material de las láminas de material depositado y añadiendo nuevas capas de estructura para formar un sistema electromecánico. La implementación de estos dispositivos ha mejorado algunas aplicaciones en antenas y ha creado formas innovadoras de cambiar los sistemas de radio frecuencia.

En esta tesis, se presentará el diseño, proceso de fabricación y la caracterización de una antena reconfigurable basada en tecnología de RF MEMS. El proceso de fabricación se llevará a cabo en el laboratorio de empaque del Air Force Research Laboratory en Wright Patterson Air Force Base, Ohio. La antena fue simulada en CST Microwave Studio. Las líneas de actuación de los conmutadores serán fabricadas para que afecten lo menos posible el comportamiento de la

antena. La antena se alimentará por medio de cable coaxial a través del plano de tierra y sustrato. La integración de los conmutadores se hará por medio de soldadura de ultrasonido. La meta final es tener la capacidad de sintonizar la frecuencia de la antena usando RF MEMS. Los patrones de irradiación se estudiarán para propósitos de caracterización.

Declaratoria de derechos de autor

Esta tesis, titulada DESIGN, FABRICATION AND CHARACTERIZATION OF A RF MEMS BASED RECONFIGURABLE ANTENNA[©] por Rey Alberto Febo 2009, fue realizada con el propósito de contribuir con el conocimiento y entendimiento de algunos principios en el campo del diseño de antenas reconfigurables que envuelven RF MEMS “switches”. Por consiguiente, otorgo permiso a la biblioteca para que reproduzca la misma para uso académico.

*All gave some,
some gave all...*

*To all who gave their lives in the search of freedom.
May they never be forgotten.*

ACKNOWLEDGEMENT

This thesis was completed after two internships in the Air Force Research Laboratory at Wright Patterson Air Force Base, Ohio. During the first internship, Dr. Nelson Sepúlveda worked on the design of the antennas that were going to be used as a proof of concept for reconfigurable antennas. On the second one, I had to learn how to learn...

During the first year of graduate school I learned the basics in electromagnetic theory. I thank Dr. José Colom Ustariz and Dr. Sandra Cruz Pol for giving me these first lessons, and for helping establishing a very good comradeship between the electromagnetic students. The social gathering they put together at their home were very refreshing. Also, they allowed me to use the CASA facilities even though I wasn't part of their research group. Thanks to Dr. Rafael A. Rodríguez Solís for motivating me to go into designing antennas. I want to specially thank Alix for teaching me the basics in antenna arrays. I also received great support from Dr. Félix E. Fernández and Armando Rúa at the physics department with thin films. Thanks for sharing your knowledge, time and equipment. I couldn't have finished without the support of Dr. Nelson Sepúlveda. Thanks for putting up with me and my personal projects and for not giving up on me.

My transition from Puerto Rico to Ohio was smooth thanks to Nivia Colón-Díaz and Jorge Villa Girón. They let me stay at their home and provided transportation until I was set up. Their friendship is one of my most cherished treasures.

During the tenure of the second internship, I was able to talk to world known experts in the antennas, materials and MEMS fields. I was given access to multimillion dollar class-100 clean room and one of the most sophisticated anechoic chambers. I want to thank Ms. Jacqueline Toussaint for giving me this opportunity and for believing in me. Special thanks to Dr. John L. Ebel for spending many hours helping me with the concept evaluation to meet design goals and refining the RF MEMS switches implementation into the antenna design. Some other people assisted when their expertise was needed: Mr. Thomas Dalrymple with guidance on manufacturing issues and materials selection, Mr. Nathan Kornbau and David Kuhl at Radio and Scattering Compact Antenna Laboratory with the evaluation on design feasibility and measurements in the anechoic chamber, Dr. Bradley Kramer and Kyle Zeller with modeling and

simulations in CST Microwave Studio, Jorge Villa and Ryan Chilton on EM simulation concepts, and Mr. Larry Callahan from Wyle Labs in the wire bonder.

Nobody can live a happy live without an abundance of love shared with family and friends: my mother Gladys, my sisters Lizbeth and Jenisa, my brother Carlos, Titi Tute, Tío Luis, Pichi and family, Alexis and Rosita, Titi Chiqui, Tío Vitín, Tato (“el Compai”), Víctor, Viviana, Titi Tere, the wise Tío Gelo, Mily, Ramón, Joya, Militza, Memi, Jualy, Jazmin, my right hand Jomar, and Sasha.

And the most important person in my life, my beautiful wife Janice; she followed my steps during 10 and a half years in the Marine Corps and during my studies. Her support will always be her biggest gift to me and my career.

Table of Contents

LIST OF TABLES	xii
LIST OF FIGURES	xiii
CHAPTER I: Research Motivation and Goal	1
1.1 Introduction	1
1.2 Thesis objective	2
1.3 Overview of this Thesis	3
CHAPTER II: Antenna Theory and Design	5
2.1 Microstrip antenna technology	5
2.2 Microstrip material	7
2.2.1 Fringing field and effective dielectric constant	8
2.2.2 Material losses	12
2.2.3 Substrate effect – solid state explanation	13
2.2.4 Skin depth	14
2.3 Rectangular patch	16
2.3.1 Radiation pattern of rectangular patch	18
2.4 Feeding techniques and input impedance	19
2.4.1 Probe feed	20
2.4.2 Microstrip feed	22
2.4.3 CPW feed	23
2.5 Frequency response and impedance bandwidth	23
2.6 Spiral Antenna	24

2.7 Coupled Microstrip Patches	25
2.8 Chapter Conclusions	25
CHAPTER III: Reconfigurable Antennas	26
3.1 Reconfigurable antennas	26
3.2 Reconfigurability concept	27
3.2.1 Frequency Reconfigurability	27
3.2.2 Radiation Pattern reconfigurability	28
3.3 RF-MEMS based reconfigurable antennas – previous designs	28
3.4 Recent trends	35
3.5 Design tradeoffs	35
3.6 Chapter conclusions	36
CHAPTER IV: Methodology	37
4.1 Purpose	37
4.2 Proof of Concept and Selection of Material	38
4.2.1 Procedure	40
4.3 Simulation Software	40
4.4 Proposed Antenna Designs	41
4.4.1 Reconfigurable Microstrip Patch Antenna	42
4.4.1.1 Theoretical Design of the Main Patch	42
4.4.1.2 Coupled Microstrip Patches	44
4.4.1.3 Design of Patch Extensions, Hypothesis and Constraints	44
4.4.2 Additional Reconfigurable Antenna Designs	45
4.4.2.1 Spiral Antenna Design	45

4.5 Chapter Conclusions	46
CHAPTER V: Results and Discussions	47
5.1 Proof of Concept	47
5.1.1 Antenna System	47
5.1.2 Problems Encountered and Lessons Learned	48
5.1.3 Results and Discussions	50
5.1.4 Conclusion of Proof of Concept	56
5.2 Switch Characterization	56
5.2.1 Operational Principle	57
5.2.2 Switch Characterization System	57
5.2.3 Results and Discussions	59
5.2.4 Integration with the Antenna	63
5.3 Reconfigurable Microstrip Patch Antenna Design	65
5.3.1 Design of Main Patch	66
5.3.2 Design of Patch Extensions	68
5.3.3 Simulations and Results	70
5.3.4 Fabrication	79
5.3.5 Results and Discussions	82
5.4 Additional Reconfigurable Antenna Designs	83
5.4.1 Spiral Antenna	84
CHAPTER VI: Conclusions and Recommendations	89
6.1 Conclusions	89

6.2 Recommendations	92
References	93

List of Tables

Table 2.1 Skin depth of commonly used metals.	15
Table 5.1 Operating frequency bands for the configurations of monopole-loop antenna.	50

List of Figures

Figure 1.1	Thesis Overview	4
Figure 2.1	Common shapes of microstrip patch antennas.	6
Figure 2.2	Microstrip material structures.	7
Figure 2.3	EM field lines not contained within the substrate in transmission lines.	9
Figure 2.4	E-field in microstrip material.	9
Figure 2.5	Effect of fringing in electrical dimension of a patch antenna.	10
Figure 2.6	Transmission line model. [18]	13
Figure 2.7	Rectangular microstrip antenna [2].	16
Figure 2.8	(a) Cross section of a probe fed patch antenna.	
	(b) Principal plane radiation patterns of a microstrip antenna. [23]	19
Figure 2.9	Equivalent circuit for probe-fed microstrip antenna. [28]	21
Figure 2.10	Probe fed rectangular microstrip patch antenna. [29]	21
Figure 2.11	(a) Microstrip line feed. [32]	
	(b) Inset feeding. [30]	
	(c) CPW fed antenna [33]	22
Figure 2.12	Single-arm square spiral antenna (a) top view and (b) side view.	24
Figure 3.1	Design characteristics of the Sierpinski gasket antenna. [49]	29
Figure 3.2	Picture of 3x3 array prototype fabricated on 0.125” thick substrate [48].	31
Figure 3.3	Fabricated antenna with Radant MEMS switches [50].	32

Figure 3.4	Reconfigurable Scan Beam Single-Arm Spiral Antenna [51].	32
Figure 4.1	Monopole-folded monopole antenna.	38
Figure 4.2	Proposed layout for the reconfigurable microstrip patch antenna.	42
Figure 4.3	Proposed reconfigurable single-arm square spiral antenna.	46
Figure 5.1	Monopole-folded monopole (a) layout and (b) photograph after assembly.	48
Figure 5.2.	Return loss of the monopole-folded monopole in the Off-Off switch configuration.	51
Figure 5.3	Simulated radiation patterns at 14.25 and 15.425 GHz.	51
Figure 5.4	Return loss of the monopole-folded monopole in the On-On switch configuration.	52
Figure 5.5	Simulated radiation patterns of monopole-loop at 13 GHz, 15 GHz and 17 GHz.	52
Figure 5.6	Return loss of the Off-Off and On-On states of the switches combined.	53
Figure 5.7	Return loss of the Off-On and On-Off states of the switches.	53
Figure 5.8	Gain vs frequency of the monopole-loop before actuating the switches.	54
Figure 5.9	Radiation pattern from 7-12 GHz in azimuth cut.	55
Figure 5.10	Radiation pattern from 13-18 GHz in azimuth cut.	55
Figure 5.11	System used for switch characterization.	58
Figure 5.12	Test configuration for Radant-RF MEMS switch with microstrip to CPW adapters used for switch characterization.	58

Figure 5.13	(a) Return loss and (b) insertion loss vs frequency under different actuation voltages.	59
Figure 5.14	Switch model for RMSW101 version.	60
Figure 5.15	Return loss of the Off-Model compared to the measured return loss of the switch.	60
Figure 5.16	Return loss of the On-Model compared to the measured return loss Of the switch.	61
Figure 5.17	Isolation of the switch compared to the switch model.	61
Figure 5.18	Isolation phase of the switch compared to the switch model.	62
Figure 5.19	(a) RF-MEMS switch used in the antenna subsystem and (b) the protection circuit recommended for safe dissipation of the charge build-up [65].	63
Figure 5.20	Measurement of radiation pattern for azimuth angle.	65
Figure 5.21	Top view of Main Patch.	66
Figure 5.22	4 Patches in parallel simulated as hard wire modeling.	69
Figure 5.23	The real impedance of 4 patches in parallel.	70
Figure 5.24	Microstrip patch showing the E-field intensity out of the radiating edges.	71
Figure 5.25	E-field lines entering and exiting the microstrip patch.	72
Figure 5.26	(a) S11 plotted in a Smith Chart from 9-11 GHz. (b) S11 dB-parameter shows resonance at 10 GHz.	72 73
Figure 5.27	Expected radiation pattern of the microstrip patch (a) without actuation of switches at 10 GHz	73

	(b) then in phi plane cut,	73
	(c) and in the theta plane cut.	74
Figure 5.28	The proposed microstrip patch layout (a) without the RF MEMS switches and (b) with the switches embedded in the modeling.	75
Figure 5.29	Return loss of antenna with additional patches integrated.	76
Figure 5.30	Final wiring of the switches.	76
Figure 5.31	S11 for the reconfigurable microstrip patch antenna with hard wire modeling of the switches.	77
Figure 5.32	VSWR of the reconfigurable microstrip patch antenna.	77
Figure 5.33	Real part of the input impedance.	77
Figure 5.34	Return loss of antenna with switches in On-On state for 8-18 GHz.	78
Figure 5.35	Machinery used in the fabrication of the antennas.	80
Figure 5.36	Integrated microstrip patch antenna.	82
Figure 5.37	Return loss as a function of frequency of the reconfigurable microstrip patch with actuation of the switches.	83
Figure 5.38	Return loss as a function of frequency of the reconfigurable spiral antenna in the monopole configuration.	84
Figure 5.39	Return loss as a function of frequency of the reconfigurable spiral antenna in the monopole configuration plotted in Smith Chart.	85
Figure 5.40	Return loss of spiral configuration as a function of frequency.	86
Figure 5.41	Return loss as a function of frequency of the reconfigurable spiral antenna with one switch simulated in “On” state plotted in Smith Chart.	86
Figure 5.42	Integrated monopole-spiral antenna.	87

Chapter 1

Research Motivation and Goals

1.1 Introduction

The theory, design and technology development of radio frequency microelectromechanical systems (RF MEMS) are the subject matter of much research in the past few decades. They are still a work in progress, and as it comes along, the amount of applications and fields that MEMS have influenced in has stirred the research interests of several organizations in the United States government and other countries, and has driven many companies to change their organization, resource assignments, and goals. Researchers are still looking for applications for what already has been designed, searching for improvement in power handling and reliability, and coming up with new ideas for next generation communication systems in order to satisfy an increasing need to operate in network systems with different standards and operating frequencies. This need for wireless communication has forced the creation of tunable and reconfigurable devices all around the electronics and electromagnetic fields.

The implementation of these new devices has particularly improved some applications in the antennas world and has created innovative ways of changing the current RF systems. The capability of tuning an antenna in order to have multiple resonant frequencies is one of them. With the application of RF MEMS switches and resonators, researchers have been able to change the topology of an antenna, thus changing its resonance frequency, and to steer electrically where the antenna beam is pointing at by changing and controlling the polarization of an antenna array with the activation of different sections of such array. These are just some examples of what is in

the design table to provide more efficient ways of using the available bandwidth and to achieve a higher data transmission rate for an increasing amount of users.

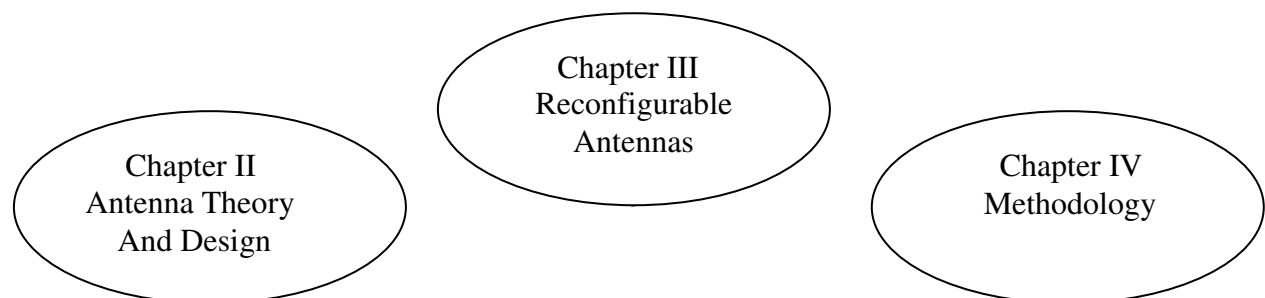
1.2 Thesis Objective

The goal of a reconfigurable antenna is to reduce the complexity of an antenna system operating over a wide frequency band, and to reduce the need of multiple antennas to perform a specific task, providing a relatively large bandwidth and achieving a dynamical reconfiguration within a few microseconds. They serve different applications at different frequency bands, such as communications in the L-band (1-2 GHz) and synthetic aperture radar (SAR) at X-band (8-12 GHz). The focus of this thesis is to design an antenna that is able to reconfigure within the X-band, which could support in the future several platforms, which may include satellite or UAV-based communications and radar applications (SAR, terrain mapping, GMTI, AMTI, etc.). The design, simulation, fabrication and characterization of a multiband reconfigurable antenna are presented in this thesis. The design of a proof of concept for previous work done with MEMS based reconfigurable antenna designs with off-the-shelf components is presented as well. The major accomplishments and contributions to the scientific community reported in this thesis include:

1. The characterization and integration of off-the-shelf RF MEMS switches in the design of a reconfigurable antenna that covers several frequency bands.
2. The implementation of biasing techniques with the lowest effect possible in the radiation pattern of the antenna.
3. The exploration of future applications for the designed antenna array, to include civilian and military applications.

1.3 Overview of the Thesis

This thesis presents the design, fabrication, and characterization of an RF MEMS-based reconfigurable antenna to be used at different operating frequencies, thus reducing the complexity of implementing several antennas and circuitry for different applications. Chapter 2 explains the theory of microstrip antenna technology and antenna arrays. Some feeding techniques and matching networks are studied, along with the effects of specialized substrate materials such as frequency selective surfaces. It also discusses the research being conducted by different researchers in the topic of reconfigurable antennas based on RF MEMS technology, along with recent trends in the technology. The third chapter describes the methodology used in the fabrication of the RF-MEMS based reconfigurable antenna (successful and unsuccessful attempts), the type of feed structure used, and the integration of the RF MEMS switches. Then, in chapter four, the results are discussed. The details for the design and fabrication challenges of the antenna structure are presented. In the last chapter the conclusions are drawn and some recommendations are made for future designs.



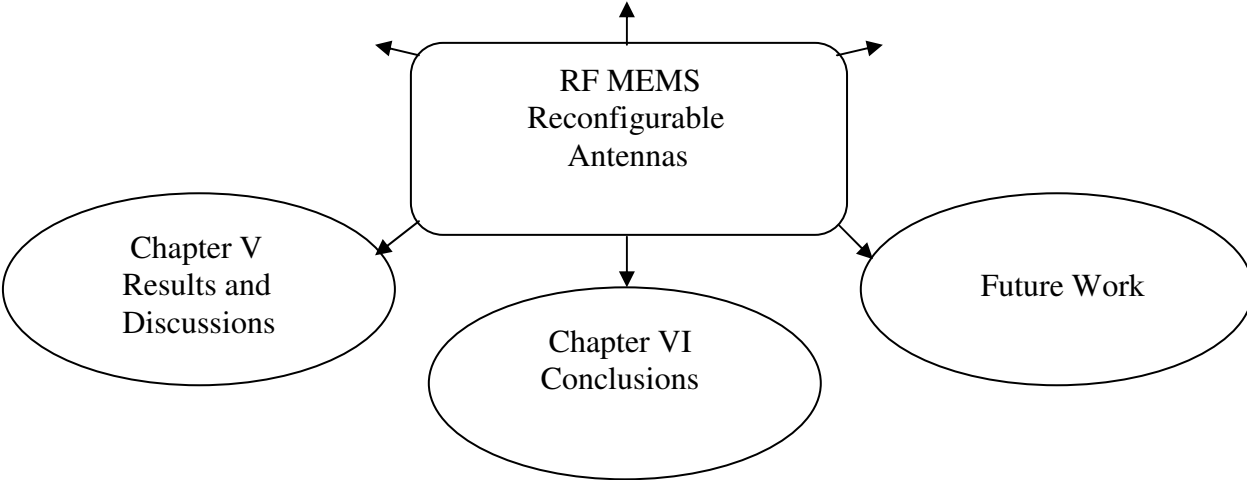


Figure 1.1 Thesis Overview

Chapter 2

Antenna Theory and Design

2.1 Microstrip Antenna Technology

Microstrip antennas are the most commonly used structure due to their highly desirable physical characteristics such as light weight and low volume, low profile (can be easily made conformal to host surface), low cost (can be manufactured in large quantities), ruggedness (when mounted on rigid surfaces), linear and circular polarization capability, dual and triple frequency operations capability, and ease to form large arrays with (spaced at half-wavelength or more). [1] They can also be shaped to form curved surfaces (conformal structures are possible). They are well suited to integration with integrated circuits and monolithic microwave integrated circuits (MMICs). However, they have some disadvantages that the designer must consider. For example, they have limited bandwidth (usually 1 to 5%), high feed network losses, low power handling capacity, poor cross polarization, spurious feed radiation (side lobes and cross polarization), surface wave excitation, and tolerance problems. [1-2] Much of the work done in microstrip antenna designs has thus gone into trying to overcome these problems in order to satisfy increasingly stringent system requirements. However, this comes at the cost of increased system complexity.

The microstrip antenna was first proposed by G. A. Deschamps in 1953 [3], but didn't become practical until the 1970's when low loss soft substrate materials were just becoming available. The size of a microstrip antenna is inversely proportional to its frequency. Microstrip patch antennas don't make sense at frequencies lower than microwaves because of the required

sizes. A microstrip antenna capable of receiving FM radio at 100 MHz would be on the order of 1 meter long (which is a very large circuit for any type of substrate). For AM radio at 1000 KHz, the microstrip patch would be the size of a football field. It is more practical to see these types of antennas at the X-band (even though you see them deployed at L-band and S-band in GPS receivers and cell phones), where its size is on the order of 1 centimeter long. One application where microstrip patches are used is in satellite radio receivers (XM and Sirius). The antenna is often mounted in a vehicle and generally the angle in the X-Y plane relative to the satellite is not fixed. Thus circular polarization is employed for satellite radio so that the angle between the patch and the satellite doesn't matter.

There are some commonly used shapes in order to simplify analysis and performance prediction. These are square, rectangular, dipole, circular, triangular, circular ring, and elliptical among others (see Figure 2.1).

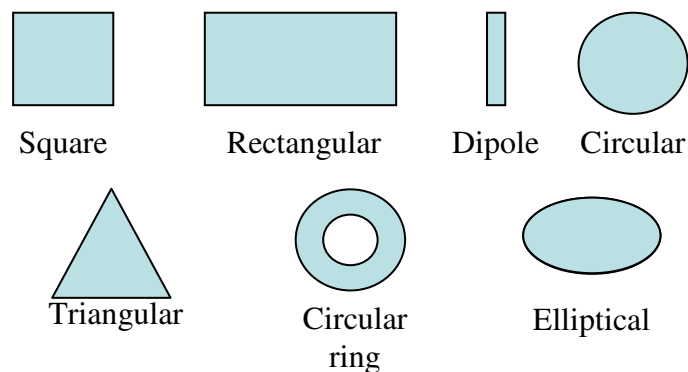


Figure 2.1 Common shapes of microstrip patch antennas.

Different designs with different configurations and feeding techniques could be employed, but one has to consider the material where they are designed. The selection of the material to be used is critical for antenna's performance.

2.2 Microstrip Material

Microstrip material consists of a sandwiched thin substrate between two conducting layers as shown in Figure 2.2. The upper conductor is the resonant structure associated with the feed network. The lower conductor is the ground plane. A microstrip antenna consists of a conducting patch etched on that upper conducting layer. The dimensions of the patch depend on the operational frequency and the substrate parameters. The substrate on which an antenna is built on has an enormous effect on the antenna behavior. It affects the resonance frequency, along with the bandwidth, and the input impedance. The amount of fringing around the patch is directly proportional to the height of the substrate. The appropriate selection of substrate thickness and the dielectric constant will lead to a low loss designs [4].

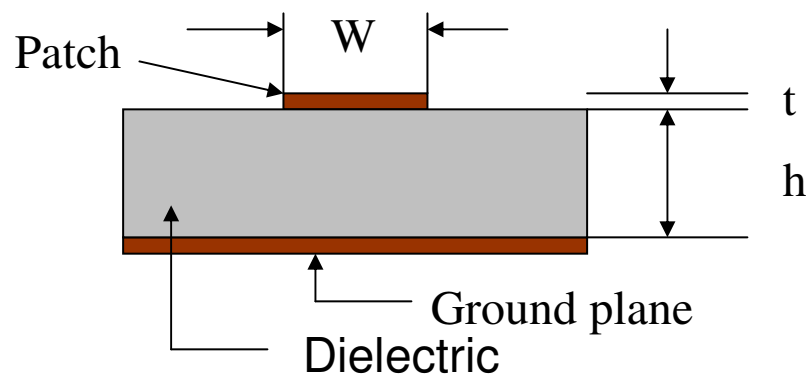


Figure 2.2 Microstrip material structure.

There are some losses associated with this type of material, which determine the antenna efficiency. The dielectric loss is specified by its loss tangent and the conducting loss by the patch conductivity (or equivalently by its skin-depth at a given frequency). [5]

2.2.1 Fringing Field and Effective Dielectric Constant

The dielectric constant (or relative permittivity = ϵ_r) of a material can be used to quantify how much a material slows an electromagnetic signal. The velocity of the signal (v) within any transmission line can be computed by:

$$v = c / \sqrt{\epsilon_r}, \quad \text{where } c = 2.998 \times 10^8 \text{ m/s (speed of light in free space)}. \quad (2-1)$$

It is also mistakenly referred to as the phase velocity, which is the rate at which the phase of the wave propagates in space [6]. Since the wavelength is proportional to the velocity of the electromagnetic signal, the electrical length of the antenna is larger in low permittivity substrates. Here is the reason why high permittivity substrates (such as GaAs with $\epsilon_r=12.9$) are employed in microwave components, to reduce their size [7], but in antennas, unless space is at a premium, you do not want to use high permittivity substrates. The way in which the electromagnetic wave propagates in the media affects the design of the microstrip structure. In order to calculate the half wavelength for the antenna design, the calculation of the effective dielectric constant (ϵ_{r_eff}) is needed. This parameter controls the resonance of the antenna. In microstrip media, most of the electric field is constrained within the substrate, but a fraction of the total energy exists within the air above the board. This means that the electromagnetic field lines are not entirely contained within the substrate (see Figure 2.3). This effect is known as fringing. The effective dielectric constant accounts for the fringing and the wave propagation in the line. Therefore, the propagating mode in the microstrip line is not a pure transverse electromagnetic (TEM) mode but a quasi-TEM.

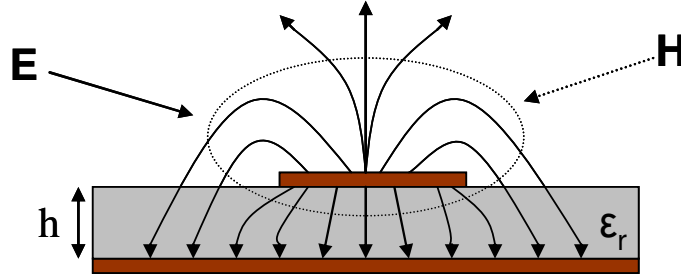


Figure 2.3 EM field lines not contained within the substrate in transmission lines.

The phase velocity in the microstrip line is given by [8]:

$$v_p = \frac{c}{\sqrt{\epsilon_{r-eff}}} \quad (2-2)$$

Since the phase velocity changes, the wavelength also changes:

$$\lambda_r = \frac{v_p}{f} = \frac{c}{f\sqrt{\epsilon_{r-eff}}} = \frac{\lambda}{\sqrt{\epsilon_{r-eff}}} \quad (2-3)$$

The fields at the edges of the patch undergo fringing since the patch dimensions are finite along the width and length (Figure 2.4). The E-plane fringing is a function of the ratio of the length of the patch to the height of the substrate (L/h) and the dielectric constant of the substrate. Since this ratio in microstrip antennas (L/h) is much greater than 1, the fringing is reduced. The same applies for the width.

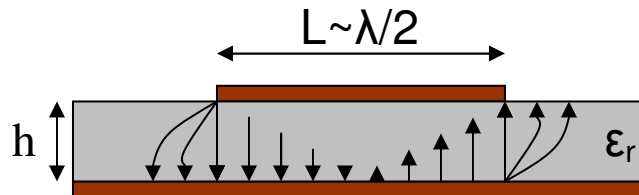


Figure 2.4 E-field in microstrip material.

The reason why the fringing affects the structure dimensions is because it makes the microstrip antenna look larger electrically by a ΔL compared to its physical dimensions [9]-[12], reducing its resonant frequency (Figure 2.5). This ΔL can be computed using equation (2-4).

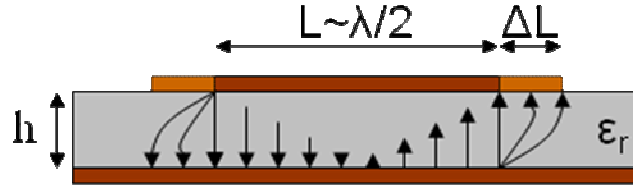


Figure 2.5 Effect of fringing in electrical dimension of a patch antenna.

$$\Delta L = 0.412h \frac{(\epsilon_{eff} + 0.3) \left(\frac{W}{h} + 0.264 \right)}{(\epsilon_{eff} - 0.258) \left(\frac{W}{h} + 0.8 \right)} \quad (2-4)$$

To perfectly match most systems, the antennas are designed to have a 50Ω input impedance (Z_{in}). The input impedance of the antenna can be adapted by varying the position for the feeding point [2], [10]-[13]. Its maximum value is at the patch border and decreases as we move inside according to:

$$Z_{in} = Z_{max} \cos^2 \left(y \frac{\pi}{L} \right) \quad (2-5)$$

Several feeding techniques will be addressed in section 2.4.

The effective dielectric constant is in the range of $1 < \epsilon_{r_eff} < \epsilon_r$. This parameter is also a function of frequency. As the operating frequency increases, the electric field concentrates in the substrate, and the effective dielectric constant approaches the value of the dielectric constant of

the substrate. For applications where ϵ_r is much greater than unity, the value of ϵ_{r_eff} will be closer to the actual value of the substrate (ϵ_r). For low frequencies the effective dielectric constant practically does not change [10]. The change in this parameter can be observed at medium frequencies, where its value increases and eventually approaches the value of the dielectric constant of the substrate. Since the transmission lines in microstrip are not entirely in the TEM mode they tend to be dispersive. That is, the effective dielectric constant and the impedance vary with the frequency of the transmitted signal. The effect is especially pronounced when the frequency is near the TEM cutoff frequency [14].

At low frequencies, the effective dielectric constant for $W/h \geq 1$ is given by:

$$\epsilon_{r_eff} = \frac{\epsilon_r + 1}{2} + \frac{\epsilon_r - 1}{2} \frac{1}{\sqrt{1 + 12 \frac{h}{W}}}, \quad (2-6)$$

and by:

$$\epsilon_{r_eff} = \frac{\epsilon_r + 1}{2} + \frac{\epsilon_r - 1}{2} \left[\frac{1}{\sqrt{1 + 12 \frac{h}{W}}} + 0.04 \left(1 - \left(\frac{W}{h} \right) \right)^2 \right], \quad (2-7)$$

for $W/h < 1$.

This analysis and equations are based on the transmission line model. Equation (2-7) is not considered for the analysis of the patch antenna, but could be used in the study of the RF behavior of biasing lines for the RF MEMS switches. These equations assume a negligible strip

thickness (t). In reality, the thickness of the strip has some bearing on the electrical performance, and the strip thickness affects the microstrip characteristics. However, for a thickness to height ratio (t/h) less than or equal to 0.005, the agreement between experimental and theoretical results obtained by assuming t/h = 0 is considered acceptable by field experts [13].

Once the effective dielectric constant is obtained, there are formulas that allow calculating the impedance of a transmission line or patch and their effective length.

For $W/h \geq 1$, the characteristic impedance can be calculated using: [15]

$$Z_0 = \frac{120\pi}{\sqrt{\epsilon_{r_eff}} \left(\frac{W}{h} + 1.393 + \frac{2}{3} \ln\left(\frac{W}{h} + 1.44\right) \right)} \quad (2-8)$$

and for $W/h < 1$,

$$Z_0 = \frac{60}{\sqrt{\epsilon_{r_eff}}} \ln\left(\frac{8h}{W} + \frac{W}{4h}\right) \quad (2-9)$$

2.2.2 Material Losses

The attenuation constant is the attenuation of an electromagnetic wave propagating through a medium per unit distance from the source. It is the real part of the propagation constant. The losses incurred in transmitting an RF signal are associated with this attenuation constant, denoted by α , and measured in Nepers/meter. One Neper is approximately 8.7dB. The total attenuation of the signal is due to four major components: the metal loss (conduction losses in the imperfect metal), the dielectric loss tangent (dielectric losses in the substrate), the

conductivity of the dielectric, and the loss due to stray radiation (surface waves excited in the substrate). [16]-[17]

$$\alpha = \alpha_C + \alpha_D + \alpha_G + \alpha_R \quad (2-10)$$

α_C = loss due to metal conductivity

α_D = loss due to dielectric loss tangent

α_G = loss due to conductivity of the dielectric

α_R = loss due to radiation

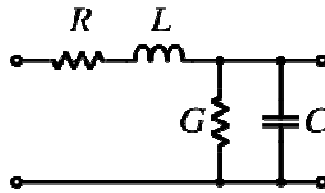


Figure 2.6 Transmission line model. [18]

2.2.3 Substrate Effect – Solid State Explanation

The electron movement at the center of the material is reduced due to a high flux density. There's an increase in the opposition to current flow in the center of the wire as frequency is increased. As the current in the center of the wire becomes smaller, most of the electrons flow is on the wire surface. When the frequency applied is 100 megahertz or higher, the electron movement in the center gets inappreciable. Therefore, the effective cross-sectional area decreases as the frequency increases. Since resistance is inversely proportional to the cross-sectional area, the resistance will increase as the frequency is increased. Similarly, since power loss increases with increase in resistance, power losses increase with an increase in frequency because of skin effect [19]-[20].

2.2.4 Skin Depth

Skin depth is a measure of the distance an alternating current can penetrate beneath the surface of a conductor. The charges within a conductive material oscillate at the same frequency as the impinging fields. The magnitude of this current, which is due to the movement of the electrons, is maximum at the conductor's surface. The current density declines proportional to the depth, which is known as skin effect. The skin depth is defined as the distance δ through which the amplitude of a traveling plane wave decreases by a factor e^{-1} and is therefore

$$\delta = \frac{1}{\alpha} \text{ in meters} \quad (2-11)$$

It can also be written as:

$$\delta = \sqrt{\frac{2\rho}{\omega\mu}} \quad (2-12)$$

where ρ = resistivity of the conductor

ω = angular frequency of the current

μ = absolute magnetic permeability of the conductor

The change in phase associated with this depth can make the current to flow in opposite direction to that on the surface. [21]

The skin depth is a property of the material that varies with the frequency of the applied wave. It can be calculated from the relative permittivity and conductivity of the material and frequency of the wave. The propagation constant, γ , is a complex number comprised of the sum

of the attenuation and phase constants, and it's related to the complex permittivity, ϵ_c , by the following equation: [21]

$$\gamma = \omega\sqrt{\mu\epsilon_c} = \alpha + j\beta, \quad (2-13)$$

where $\epsilon_c = \epsilon\left(1 - j\frac{\sigma}{\omega\epsilon}\right) = \epsilon' - j\epsilon''$ (2-14)

ϵ = permittivity of the material of propagation

ω = angular frequency of the wave

σ = electrical conductivity of the material of propagation

j = the imaginary unit = $\sqrt{-1}$

The constants can also be expressed as: [22]

$$\alpha = \omega\sqrt{\frac{\mu\epsilon}{2}\left(\sqrt{1 + \left(\frac{\sigma}{\omega\epsilon}\right)^2} + 1\right)} \quad (2-15)$$

$$\beta = \omega\sqrt{\frac{\mu\epsilon}{2}\left(\sqrt{1 + \left(\frac{\sigma}{\omega\epsilon}\right)^2} - 1\right)} \quad (2-16)$$

where μ = permeability of the material

β = phase constant of the propagating wave.

The following are some examples of commonly used metals' skin depth:

Conductor	Skin depth(μm)	Skin depth(μm)
	1 GHz	10 GHz
Al	2.529822128	0.8
Cu	2.055480479	0.65
Au	2.498199352	0.79
Ag	2.023857703	0.64

Table 2.1 Skin depth of commonly used metals

2.3 Rectangular Patch

This is the most popular type of microstrip antenna. Figure 2.7 shows the geometry of the rectangular microstrip antenna, not including the dielectric and ground plane which would be underneath. The dimension L is universally taken to mean the long dimension, which causes resonance at its half wavelength frequency. The radiating edges are at the ends of the L dimension of the rectangle, which sets up the single polarization. The radiation that occurs at the ends of the W dimension is far less and is referred to as the cross-polarization [2]. For a rectangular patch, the length L of the patch is usually $0.3333\lambda_0 < L < 0.5\lambda_0$, where λ_0 is the free space wavelength. The patch is fabricated to have a very thin t such that $t \ll \lambda_0$ (where t is the patch thickness). The height h of the dielectric substrate is usually $0.003\lambda_0 \leq h \leq 0.05\lambda_0$. The dielectric constant of the substrate is typically in the range $2.2 \leq \epsilon_r \leq 12$ [2], [10], [19], [23].

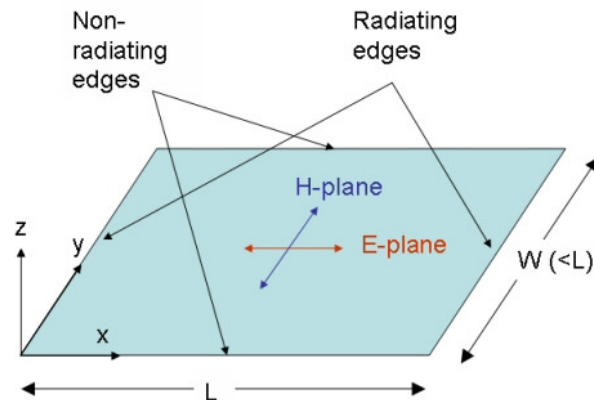


Figure 2.7 Rectangular microstrip antenna [2].

The E-field under the patch can be explained by taking a side view of the microstrip material. (See Figures 2.4 and 2.5) The fields under the L edges are of opposite polarity due to the half wave nature of the patch. When the field lines curve out and finally propagate out into

the direction normal to the substrate they are now in the same direction (both facing left). In the far field, perpendicular to the substrate, the radiation from the two sides adds up because the fields are in phase. As you look out in directions off of boresight (optical axis of a directional antenna), the intensity drops off as the fields of the two edges become farther and farther out of phase. At two angles the fields exactly cancel. Thus the microstrip patch radiation intensity depends on what direction you are facing it from (it has gain and directivity).

A few basic steps need to be followed when designing a patch antenna. First, the structure needs to be a half wavelength resonator. This parameter is controlled by the effective dielectric permittivity, which will be discussed later. In order to excite the desired TM₁₀ mode, it is imperative to make the patch length slightly less than half wavelength in the substrate (Equation 2-3), causing the parallel radiating edges to behave as two element broadside array. Second, use a low dielectric constant under the patch. This allows for a low Q factor of the magnetic wall cavity under the patch, which could also be obtained by using a thicker substrate, provides a better efficiency and larger bandwidth, but at the expense of a larger element size. Third, use a thicker dielectric than you normally would to extend the efficiency and the bandwidth, but keep in mind the height must still be just a fraction of a wavelength and that the fringing field effect will increase. It also introduces surface waves, which are not desirable since they extract power from the available power for direct radiation. Surface waves degrade the antenna pattern and polarization characteristics. There are methods that eliminate these surface waves, by introducing cavities in the design [10], [15], [19], [23].

2.3.1 Radiation Pattern of Rectangular Patch

The radiation pattern is a graphical representation of the relative electromagnetic field strength transmitted from or received by the antenna. These antenna radiation patterns are taken at one frequency, one polarization, and one plane cut (azimuth or elevation). The patterns are usually presented in polar or rectilinear form with a logarithmic strength scale. Conventionally, the patterns are normalized to the maximum graph value, 0 dB, and the directivity above an isotropic antenna is given for the antenna. In more elaborated words, an antenna radiation pattern is defined as “a mathematical function or a graphical representation of the radiation properties of the antenna as a function of space coordinates. In most cases, a radiation pattern is determined in the far-field region and is represented as a function of the directional coordinates. Radiation properties include power flux density, radiation intensity, field strength, directivity phase or polarization.” [24]

Considering a basic rectangular microstrip patch antenna with probe feeding (see Figure 2.8 (a)), let us explain the basic operation and electrical characteristics of a microstrip patch antenna. The antenna transmit mode occurs when the antenna is driven by a voltage between the probe feed and the ground plane. The electrical field components parallel to the ground plane must be very small throughout the substrate, given that the substrate is usually thin ($h \sim 0.05 \lambda_0$). This excitation will produce a current on the patch, and a vertical electrical field between the patch and the ground.

As mentioned before, the antenna will resonate around its half wave length, leading to relatively large electric field and current amplitudes. The radiation can be viewed as being generated by the induced surface current density ($J = \tilde{n} \times H$) on the patch in the presence of the

grounded dielectric substrate. The equivalent source produces a broadside radiation pattern [23] as shown in Figure 2.8 (b).

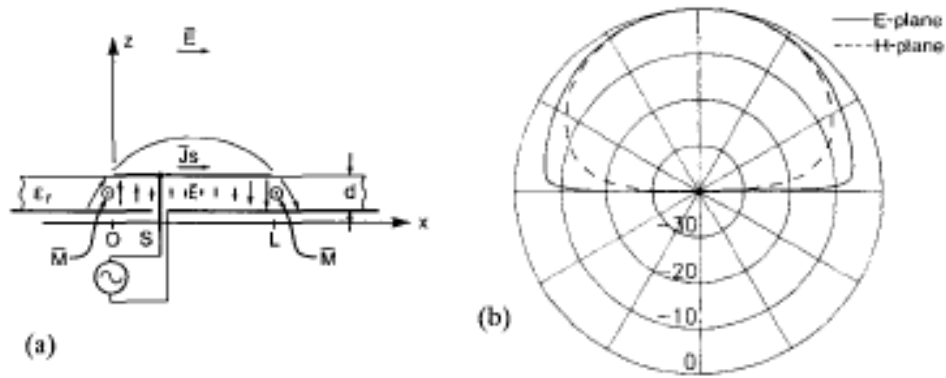


Figure 2.8 (a) Cross section of a probe fed patch antenna.

(b) Principal plane radiation patterns of a microstrip antenna. [23]

Microstrip patch antennas have shown a tendency to have radiation patterns with unwanted sidelobes and local nulls in certain directions caused by surface waves. This effect is increased in high permittivity substrate. Some researchers have removed the substrate from underneath the antenna to improve the radiation pattern, as well as to increase the efficiency and directivity [25]. This technique in combination with others is used to improve the radiation pattern and to remove the ripples presented in it.

2.4 Feeding Techniques and Input Impedance

For the antenna to be in the transmit mode, it needs to be driven by a voltage source between the probe feed and the ground plane. The reason for an appropriate feeding technique is the efficient transfer of power between the feed structure and the radiating element (impedance matching is critical) [26]. Power can be coupled into or out of the antenna by contacting and non contacting methods. The contacting feeds involved a direct contact with a transmission line,

feeding the RF power to the radiating patch using connecting elements, such as coaxial lines, microstrip lines, and coplanar waveguide (CPW). The most common techniques for non contacting methods are aperture coupling, and proximity coupling [10], [19], and [26]. Some of these methods have been used to increase the bandwidth and efficiency of the microstrip patch antennas [27]. These feeding techniques have more degrees of freedom than the contacting feeds, but this makes them harder to design. Special attention will be given to the contacting feeding techniques for “simplicity” purposes.

2.4.1 Probe Feed

A coaxial probe feeds is the termination (or connector) of a self-shielded cable used for transmission of RF signals. Probe feeds are widely used in microstrip patch antennas. The feed is the inner conductor, which extends through the dielectric and is soldered to the radiating patch, while the outer conductor is connected to the ground plane. The approximate location of the contact between the inner conductor and the patch is at a third of the way between the patch center and the radiating edge, to obtain an input impedance of 50Ω ($Z_{in}=50\Omega$). The main advantage of this type of feeding technique is that the feed can be placed at any desired location inside the patch. This technique is easy to fabricate and has low spurious radiation [28]. The contact location is at the center of the patch relative to the W side, and along the center axis of the L side of the patch. The antenna equivalent circuit is shown in Figure 2.9 and the geometry of the patch with a probe feed is shown in Figure 2.10.

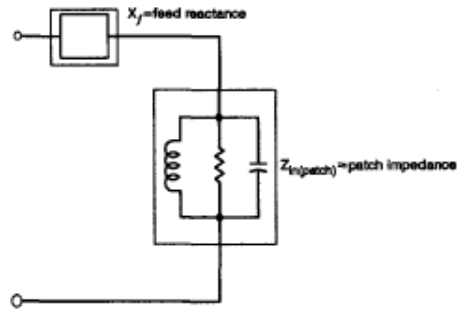


Figure 2.9 Equivalent circuit for probe-fed microstrip antenna. [28]

The input impedance of a microstrip patch antenna controls the radiated power and impedance bandwidth. The total input impedance of a probe fed patch antenna consists of the probe reactance in series with the patch impedance. The models for the probe feed appear to consider only the inductive reactance. There are two components considered by the total feed reactance, the inductive reactance of the probe plus the capacitive reactance between the patch and the ground plane [28].

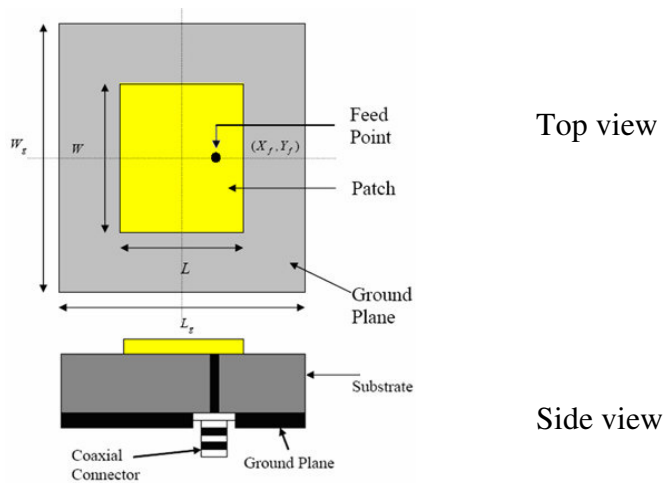


Figure 2.10 Probe fed rectangular microstrip patch antenna. [29]

The effect of the feed type and location has been widely studied and used for its ease of fabrication, but for array configurations it is preferred to use microstrip lines [30]. Even though theoretical models indicate that the resonant frequency should not be affected by the feeding technique employed when dealing with the microstrip patch, some researchers have found that there are variations up to 2%, which could be due to the tolerance errors in the patch dimensions and/or inhomogeneities in the substrate permittivity [31].

2.4.2 Microstrip Feed

In the microstrip line feed, a conducting strip smaller in width than the patch connects directly to the edge of the patch (edge feeding, see Figure 2.11 (a)). The transmission line can be etched or milled on the same substrate for better integration and to provide a planar structure. Another type of microstrip line feed is the inset feeding (Figure 2.11 (b)), which is used to match the impedance of the feed line to that of the patch without the need of an external matching network [32]. However, as the substrate thickness increases, the surface waves and spurious radiation increase as well, setting a limit on the bandwidth (typically 2-5%). The inherent asymmetry of the microstrip feed line generates higher order modes, producing cross-polarization.

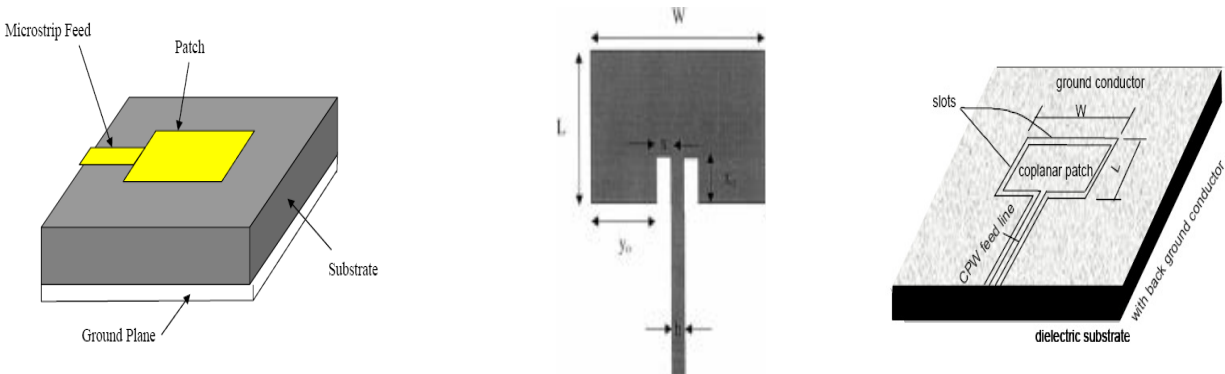


Figure 2.11 (a) Microstrip line feed. [32] (b) Inset feeding. [30] (c) CPW fed antenna [33]

2.4.3 CPW Feed

CPW fed patch antennas are normally used at microwave frequencies [33]. This structure consists of a patch surrounded by a spaced ground conductor and a CPW feed line as shown in Figure 2.11 (c). It is similar to the folded slot antenna. Other structures have been fabricated with a CPW feed line and a transition to a simple printed transmission line.

2.5 Frequency Response and Impedance Bandwidth

The frequency response of an antenna is defined as its variation (or stability) of the input impedance over frequency. The complex input impedance ($Z_{in}(\omega) = R(\omega) + jX(\omega)$ form, with $\omega = 2\pi f$ - angular frequency) provides the ability to consider the antenna as a circuit element. The input impedance of the antenna element can be used to determine the reflection coefficient (Γ) and then to calculate other related parameters, such as voltage standing wave ratio (VSWR) and return loss (RL), as a function of frequency [34].

$$\Gamma = \frac{Z_{in} - Z_0}{Z_{in} + Z_0} \quad (2-17)$$

$$VSWR = \frac{V_{max}}{V_{min}} = \frac{1 + |\Gamma|}{1 - |\Gamma|} \quad (2-18)$$

$$RL = -20 \log |\Gamma| \quad (\text{dB}) \quad (2-19)$$

The impedance bandwidth of a patch antenna is strongly influenced by the spacing between the patch and the ground plane. As the patch is moved closer to the ground plane, more energy is stored in the patch capacitance and inductance and less energy is radiated (the Q of the antenna increases) [35]. The Q factor is a dimensionless parameter that compares the time constant for decay of an oscillating physical system's amplitude to its oscillation period. A higher

Q indicates a lower rate of energy dissipation relative to the oscillation frequency, so the oscillations die out more slowly. A good antenna design should strive for a low Q factor. A very rough estimate of the bandwidth is:

$$\frac{\delta f}{f_r} = \frac{Z_0}{2R_{rad}} \frac{h}{W} \quad (2-20)$$

where h is the height of the patch above the ground plane, W is the width (near a half-wavelength), Z_0 is the impedance of free space, and R_{rad} is the radiation resistance of the antenna.

2.6 Spiral Antenna

Spiral antennas are a class of antenna that are rotational symmetric. They are attractive because of the broad bandwidth, circular polarization and wide radiation beam width [36]. The arm length determines the resonance frequency of the antenna. The radiation is perpendicular to the plane of the antenna. Making the spiral into a square will degrade this performance since there will be discontinuities in the rotation symmetry. This is due to the corners and the parallel nature of the turns.

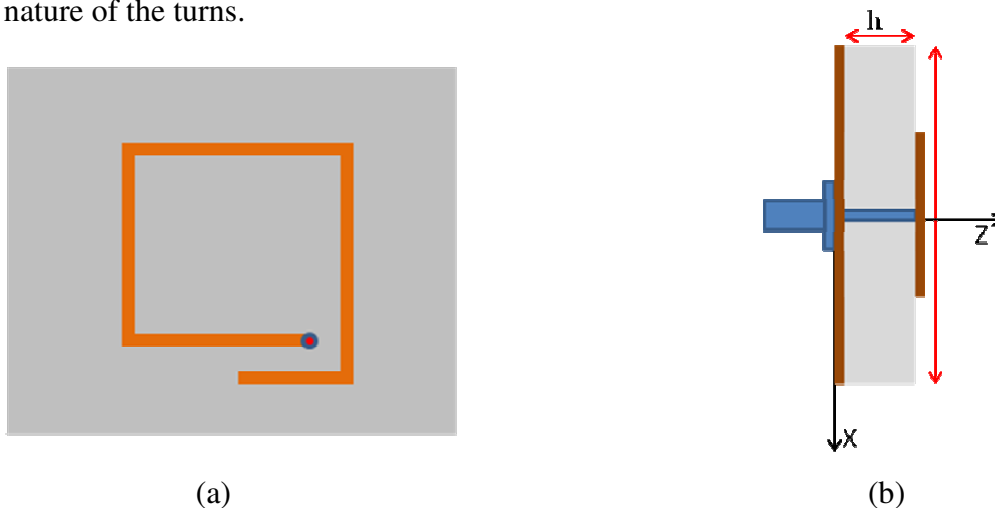


Figure 2.12 Single-arm square spiral antenna (a) top view and (b) side view.

A single-arm square spiral microstrip antenna can be design to start as a small monopole, then reconfiguring to the spiral configuration. Figure 2.12 shows a top and side view of this antenna. The reconfigurable spiral antenna is expected to demonstrate the frequency tuning and radiation pattern changing capabilities.

2.7 Coupled Microstrip Patch

Microstrip patches can couple with radiating surfaces in close proximity, acting as parasitic elements. This technique relies on the mutual coupling between closely spaced driven and parasitic elements, resulting in effective array behavior from a single feed point. This method provides isolation of the driven element from the tuned element or elements until actuating the switching device or devices. Wide-frequency bandwidth and a range of available topologies and functionalities can be achieved [34]. Therefore, changes in radiation patterns are achieved through changes in the coupling between the elements, which, in turn, change the effective source currents on both the driven and parasitic elements.

2.8 Chapter Conclusions

This chapter presents a literature review of the most commonly used microstrip antenna structures, their most suitable feeding technique, as well as a rough explanation of the substrate effects over the antenna performance. The results of previous investigative works were introduced, as well as the literature of the antenna structure to be designed.

Chapter 3

Reconfigurable Antennas

3.1 Reconfigurable Antennas

Reconfigurable antennas have become more attractive with the increased demand for multiband antennas. They provide more levels of functionality to a system by eliminating the need for complicated wideband antenna solutions. Common antenna designs not involving reconfigurability impose restrictions on the system performance because of their fixed structure. Reconfiguring antennas can enhance their performance by providing the ability to adapt to new operating scenarios.

There are several methods that rely on geometry reconfiguration for the tuning of the operating frequency of a particular antenna design, including varactor and PIN diodes, and the use of optically activated switches by fiber optic cables [37]-[39]. Many antennas have been designed to maintain their radiation characteristics by using self-similar structures, while changing the aperture dimensions for a different operating frequency [40]-[42]. Others designs consist of using a linear dipole antenna that is shortened to a specific length to operate at a higher frequency [43]. In the reconfigurable dipole case the radiation pattern stays the same because the antenna current distribution will be the same relative to the wavelength of the resonant frequency. Some reconfigurable antenna applications change the radiation pattern but maintain the same resonant frequency [44]. This concept can enhance a system's ability to null jamming, or undesirable noise sources by directing the energy to the intended user.

The challenge faced by antenna designers is that the reconfiguration of one property, for example, frequency response, will have an impact on radiation characteristics. Likewise, reconfigurations that result in radiation pattern changes will also alter the antenna's frequency response. This linkage is not desirable among antenna developers, which usually prefer the characteristics to be separable.

3.2 Reconfigurability Concept

The concept of reconfigurable antennas refers to a change in the frequency characteristics, radiation pattern, impedance bandwidth, and/or polarization of an antenna by changing its aperture dimensions or geometry through electrical or mechanical means. By tuning the operating frequency, the antenna could be used to filter signals interfering with the communication or simply to change operating frequency band [34].

3.2.1 Frequency Reconfigurability

Antennas with reconfigurable frequency response (also known as tunable antennas) can either switch abruptly from one frequency band to another or continuously perform this task. The frequency response reconfigurability is achieved by actively controlling the effective electrical length of the antenna thus enabling the antenna to operate in different frequency bands. This is usually done by adding or removing a part or parts of the antenna through electrical, mechanical, optical, or other means [37]-[42]. The antenna resonant frequency can also be altered by maintaining the antenna footprint but changing the radiating current path [45].

3.2.2 Radiation Pattern Reconfigurability

The radiation pattern reconfigurability is needed to steer the radiation pattern away from noise sources or to reduce interference. To reconfigure the radiation pattern, some researchers have used shorting pins and in-line open tuning elements [44]. Possible applications for this type of antennas are in phased antenna arrays in wide-angle scanning.

There are methods to change radiation patterns independently from frequency behavior. One of these methods is the use of electrically tuned or switched parasitic elements. This method provides isolation of the driven element from the tuned element or elements, potentially wide-frequency bandwidth, and a range of available topologies and functionalities [34]. This technique relies on the mutual coupling between closely spaced driven and parasitic elements, resulting in effective array behavior from a single feed point. Therefore, changes in radiation patterns are achieved through changes in the coupling between the elements, which, in turn, changes the effective source currents on both the driven and parasitic elements.

3.3 RF-MEMS Based Reconfigurable Antennas – Previous Designs

The concept of reconfigurable RF MEMS based antenna systems was first introduced in 1998 by E. R. Brown [46] and many researchers have enthusiastically studied this area since then. In the past, the resonant frequency of the microstrip patch antenna was tuned by adjusting the effective length of the patch using varactor diodes [47]. RF MEMS switches have replaced FETs and diodes in certain applications. They have been fabricated, tested and measured against these solid state devices and were found to have few advantages for low and medium power

handling applications [46], [48]. Nevertheless, the integration of RF MEMS switches hasn't been demonstrated and/or explained in depth.

Research groups have described different issues during the integration of the MEMS switches and the complete system. Anagnostou et al. demonstrated the concept of reconfigurable antenna design and fabrication with self-similar fractal antennas [49]. In their design, shown in Figure 3.1, they started by characterizing a single antenna element and then improving their design and fabrication process for achieving a multiple-frequency antenna. These antennas have the advantage of radiating similar patterns in a variety of frequency bands. Their design, feed, and performance as well as the structure and the biasing network of the used RF-MEMS switches were the primary objective of the research. They also presented the functionality of a new type of RF-MEMS based reconfigurable multiband antenna consisting on a self-similar design, and introduced an analytical procedure to be used in their antenna design. Even though their antenna design had good characteristics, its performance showed relatively shallow resonances, with respect to a return loss $S_{11} = -10$ dB, which they improved later.

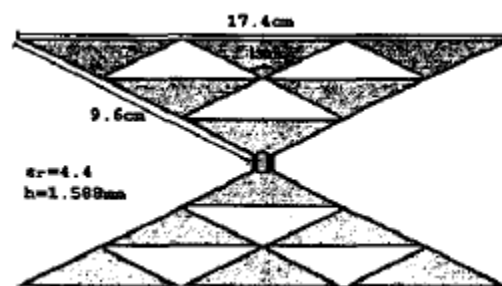


Figure 3.1 Design characteristics of the Sierpinski gasket antenna. [49]

The Sierpinski multiband fractal antenna was introduced in 1998 [41]. This antenna is described by an infinite number of iterations with an infinite number of frequency bands,

resulting in a very complex antenna structure. Their approach was to apply low pass filters between the triangle interconnections to suppress any side-lobes that may exist after the first resonance. Most of the research regarding Sierpinski antennas has been done for a low relative permittivity structure etched on thin dielectric materials, thus approximating the free space environment. Anagnostou, et al. also followed the principles of the Sierpinski antenna to design their own RF MEMS-based reconfigurable Sierpinski [42]. They implemented three sets of RF MEMS switches with different actuation voltages to sequentially activate and deactivate parts of a multiband Sierpinski fractal antenna. The direct actuation of the electrostatic MEMS switches was done through the RF feeding line. The antenna was fabricated over a liquid crystal polymer substrate and operates at several different frequencies between 2.4 and 18 GHz. It was the first RF MEMS reconfigurable antenna on a flexible organic polymer substrate for multiband antenna applications.

Gabriel M. Rebeiz studied the use of RF MEMS switches in microstrip patch antennas and feed structures for developing reconfigurable multiband antennas [48]. He named the design reconfigurable patch module (RPM). The RPM consists of a 3x3 array of patches connected together using MEMS switches. However, the real MEMS switches were not implemented since they were not available. Instead, they simulated the MEMS switches using ideal open and closed circuits as shown in Figure 3.2. Their contribution is that they were able to achieve 12% impedance bandwidth for the L-band configuration and greater than 7% bandwidth at X-band, demonstrating that with the RPM the frequency was reconfigured from one band to another. Rebeiz also talks about the integration of RF MEMS switches as ideal elements for reconfigurable antennas in his book [43]. He does a slight comparison of them against their solid state devices counterparts, FET switches and P-I-N diodes. Chapter 13 is dedicated to the

description of reconfigurable dipole and slot antennas, reflect arrays, and some of the problems that are encountered when designing reconfigurable antenna arrays.

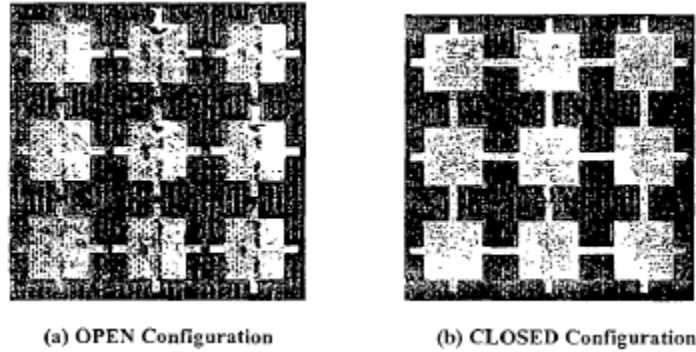


Figure 3.2 Picture of 3x3 array prototype fabricated on 0.125” thick substrate [48].

Jennifer T. Bernhard from University of Illinois at Urbana Champaign also performed much research on this field, implementing the concept of integrating packaged RF MEMS switches into a square spiral antenna by surface mounting techniques, shown in Figure 3.3 [50]. This concept will be used in this thesis, where the feasibility of implementing off-the-shelf RF MEMS switches for reconfigurable antennas will be addressed. In their research, they modified the switch to reduce the impedance mismatch, as well as the antenna to physically and electrically accommodate the switch. An electrically active single stub matching network is included in their design, but only in one of the antenna configurations. Concurrent with this previous work, a research group from University of California at Irvine, supported by DARPA and NSF, presented a reconfigurable rectangular spiral antenna with a set of MEMS switches, which were monolithically integrated and packaged onto the same substrate [51]. This system, shown in Figure 3.4, was based on a single-arm rectangular spiral antenna, capable of changing its radiation pattern. Chang won Jung, *et al.*, considered their design “the first truly reconfigurable printed antenna design using MEMS devices as active elements integrated in the

same low loss substrate". The effort of the proposed system was to emphasize the feasibility of MEMS switches integration into the same substrate for antenna applications.

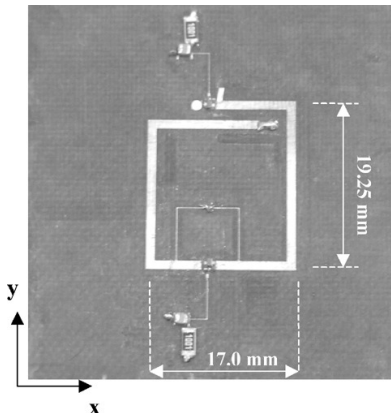


Figure 3.3 Fabricated antenna with Radant MEMS switches [50].

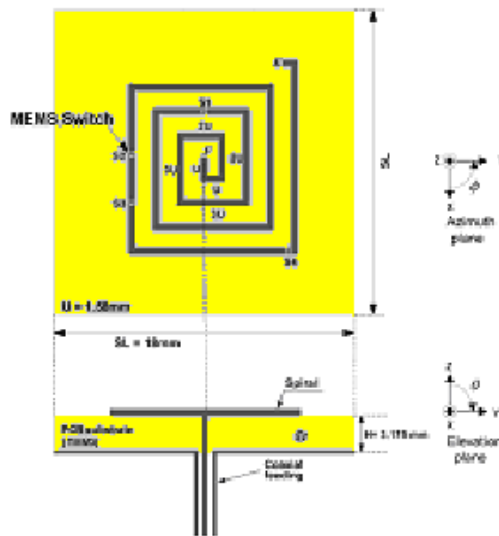


Figure 3.4 Reconfigurable Scan Beam Single-Arm Spiral Antenna [51].

Another interesting writing from a research group at Auburn University in Alabama deals with a MEMS-based electrostatically tunable circular microstrip patch antenna [52]. They designed a tunable circular microstrip patch antenna, fabricated by using printed circuit

processing techniques. The microstrip patch antenna was patterned on the top side of a Kapton polyimide film, suspended above the ground plane. The patch was inductively coupled to a coplanar waveguide (CPW) feed line via a slot in the ground plane. The only drawback to this work was that for a tuning range of 270 MHz, they needed an actuation voltage of 165 V. Previously, they were able to achieve a higher frequency range using 268 V [53]. This is considered a high voltage since there are many products in the market with actuation voltages below 100 V and with similar characteristics [54]. Because the substrate used was not compatible for fabricating MEMS switches they needed to treat them as packaged lumped components, and use surface mounting techniques.

On 2004, a novel design for a reconfigurable slot aperture antenna over a broadband substrate/feed structure was published [55]. The proposed reconfigurable aperture (RECAP) consists of interleaved crossed-slot elements for dual-polarized and broadband array operation without grating lobes. The dimensions of the array elements can be reconfigured by using radio-frequency switches, such as RF-MEMS switches or P-I-N diodes. The array elements along with the switches are integrated into the top layer of a multilayered composite structure consisting of passive, resistively loaded frequency selective surface (FSS) elements that form a broadband ground plane system. The analysis of the FSS slot array configuration and measurements that could serve as a reference in future developments of the FSS layered arrays was emphasized.

The private industry has also seen the need for the design of reconfigurable antennas in order to reduce the complexity of an antenna system for performance over a wide frequency band [56]. A work presented in 2001 describes a reflective antenna array approach that can perform time delay beam steering by using cascaded RF-MEMS switches/coplanar strip transmission line sections. They measured the RF-MEMS switches characteristics in coplanar

strip transmission line and modeled a reflected phase of five cascaded switch transmission line sections. The true-time delay switched beams were created by placing the RF-MEMS switches along the transmission lines behind the flared notch elements, where RF-MEMS switches were proposed to be the reflective elements [57]. The switches were characterized as coplanar strip elements by designing test substrates fabricated with switches placed in both shunt and series configurations, as they used coplanar strip transmission lines to eliminate the need for a balun to microstrip line.

The MEMS switches are being researched for better radiation performance for specific applications in antenna designs. A research group in University of California at Irvine designed an air bridged RF-MEMS capacitive series switches in single pole single throw (SPST) transmission lines for reconfigurable antenna applications [58]. In their design, they analyzed the RF characteristics of the capacitive series switches, measured, and compared with coplanar waveguide (CPW) and microstrip line (MSL) structures. They fabricated the series switches monolithically on a glass wafer with a spiral antenna that operates at 11 GHz in order to measure the radiation characteristics of the antenna. They concluded that the use of RF-MEMS series switch shows better performance for electric field radiation of reconfigurable antenna applications. Other researchers have designed integrated systems of antennas and MEMS on the same substrate as well [42]. The main difference between [42] and [58] is the substrate used.

These last two examples establish the basis for the research proposed in the methodology section on Chapter 3. They have proved the feasibility of RF-MEMS-based reconfigurable antennas for many applications and the research to be done in order to fulfill future communication needs.

3.4 Recent Trends

There are specific applications where reconfigurable antennas can really make an impact in the short run. As a single-element scenario, we can look at portable wireless devices, such as a cellular telephone, a personal digital assistant (PDA), or a laptop computer [34], [59]-[61]. These devices typically use single antennas, such as monopole or microstrip antennas, which may or may not have multiple-frequency capabilities. The antenna packages integrated into these devices may have two or three antennas for diversity reception on small devices to increase the probability of receiving a usable signal. Usually, only one of the antennas is used for transmission. These devices use bidirectional communication. The transmission from the portable device to a base station or other access point is the weakest part of the bidirectional communication link because of the power, size, and cost restrictions imposed by portability and physical size. If the antenna's radiation pattern could be changed, it could be redirected toward the access point and use less power for transmission, resulting in a significant savings in battery power. In the antenna array scenario, some of this technology can greatly improve performance. In planar phase array technology, reconfigurability can provide additional degrees of freedom that may result in wider instantaneous frequency bandwidths, more extensive scan volumes, and radiation patterns with more desirable side lobe distributions [34].

3.5 Design Tradeoffs

Any design tradeoffs for any project must have a balance between the capabilities provided or required and resources available. The tradeoffs are different in every application and are usually a critical aspect of the design of an antenna with specific requirements. For example, a low dielectric constant under the patch allows for a low Q factor of the magnetic wall cavity

under the patch, which could also be obtained by using a thicker substrate. Taking into consideration the fringing fields and that the substrate thickness must be a fraction of the wavelength, a tradeoff needs to be made. A microstrip patch with these characteristics provides a better efficiency and larger bandwidth, but at the expense of a larger element size. This effect could also be explained by focusing on the wavelength behavior in the medium. Wavelength is proportional to velocity of the electromagnetic signal and a high dielectric constant lowers that velocity. The electrical length of a patch antenna is approximately a half wavelength, and consequently, the electrical length of the antenna is larger in low permittivity substrates. Here's the reason why high permittivity substrates (such as GaAs with $\epsilon_r=12.9$) are employed in microwave components, to reduce their size. Thin substrates with higher dielectric constants are desirable for microwave circuitry because they required tightly bound fields to minimize undesired radiation and coupling, and lead to smaller element size, but we want to radiate! Also, the tradeoff between gain and bandwidth should be considered, as well as the robustness of the patch versus the suitable thickness for low Q designs.

3.6 Chapter Conclusions

This chapter presents the results of previous investigative works, as well as the literature of the antenna structure to be designed. Some previous research work was also included to show the trend and usefulness of this technology. In the next chapter, the materials and methodology used to accomplish this thesis research will be described. The proposed antenna structures, design process, simulation software and results will be presented. The development of a design of experiment to obtain a model of the antenna structure will be also included, as well as an explanation and test bed used to characterize the RF MEMS switch employed in the experiment.

Chapter 4

Methodology

4.1 Purpose

The antenna design process starts with designing a common geometry that can change the driving parameter that controls the frequency and a possible change in the current distribution and energy propagation in space. A different integration technique may also allow for ease of fabrication with improved results. The parts to be integrated should provide for ease of assembly with a minimum number of parts, since this is the number one driver of labor cost. Minimizing the number of parts will eventually reduce the overhead cost, the overall cost of the product, and the cost to support the subsystem if it is integrated into a major platform. Being that the antenna is reconfigurable, it is already providing for multiuse, which permits certain economies of scale and helps support the logistics aspects of the system. The antenna structure that fits all these characteristics is the microstrip patch antenna.

It is of great interest to model and experimentally verify the performance of the microstrip patch with the rest of the antenna structure that will be added by actuation of the RF MEMS switches. This process will give us a broad understanding of the antenna behavior. It can be used to determine how the feed point affects the input impedance and, consequently, the return loss. The coupling between the main structure and the different antenna extensions, and the radiation pattern should also be studied in order to better characterize the antenna behavior. The antenna design proposed will operate in the X-band, with multiple resonances a different frequency of operation because of the coupling, perhaps a higher frequency bands if higher order

modes are excited. The switch performance will also be verified across the operating frequency band. The final goal is to have a robust design of a new structure with an acceptable performance and flexibility that can be integrated into an antenna subsystem.

4.2 Proof of Concept and Selection of Material

After analyzing several antenna designs and previous work done in reconfigurable antennas, the first project was to develop a proof of concept. This antenna structure used in this experiment should change its operating frequency band upon actuation of the switches. The proposed structure is shown in Figure 4.1. It consists of a monopole antenna, with an extension to convert it into a folded monopole upon actuation of the switches, a tapered CPW feed line, and the biasing lines for the switch.

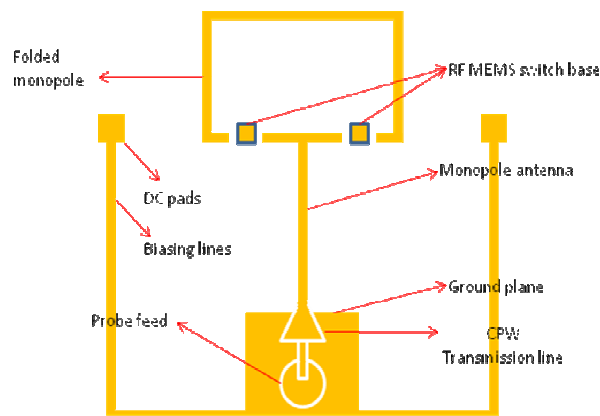


Figure 4.1 Monopole-folded monopole antenna.

The materials used in the antenna configuration were a ceramic substrate Rogers Thermoset Microwave Material (TMM®-4) with relative permittivity of $4.5 \pm 0.045\%$, thickness of 15 mils (0.381mm), with standard one sided copper cladding of $\frac{1}{2}$ oz ($17\mu\text{m}$), RF MEMS switches from Radant MEMS RMSW101TM with actuation voltage ± 100 V-dc, integrated via wire bonding with wire 7/10 mils ($17.78\mu\text{m}$) thick gold wire (1.5 mils in diameter is also

available), and a microstrip-surface mount probe feed (MSSP4847, male, full detent, right angle transition).

Since the antenna performance will be compared to previously done simulations, there are no specific dimensions to analyze or design for. The antenna layout was provided by Dr. Dimitris Anagnostou, in a partnership with Dr. Nelson Sepúlveda. The careful integration of all the components in order to fabricate a reconfigurable antenna was the focus of this effort. The design was imprinted onto the substrate with the use of a milling machine. The layout is imported in the computer that controls the milling machine, which will remove the unwanted part of the metal layer, resulting in the pattern being transferred to the substrate.

Upon finalizing the integration of the components, the end result was a monopole antenna that increased its electrical length and converted into a folded monopole by actuating the RF MEMS ohmic contact switches. This is a two bit configuration that provided four different states or configurations. The antenna has two very distinct configurations: the “Off-Off” and the “On-On” configurations. Each one is characterized by a different frequency of operation and a different radiation pattern. Two more configurations can be achieved by actuating either one of the switches by itself. However, these configurations are symmetric and do not differ significantly. The resulting antenna then has four different configurations that will provide different current distribution for different operating frequencies and radiation patterns. Principal attention was given to the “Off-Off” and the “On-On” configurations, since they provide the shift in frequency desired, and it is simple to actuate both switches at the same time with hot switching. The “Off-Off” configuration is essentially a top-hat monopole with 8.2mm length and 4.7mm of total loading in order to lower its resonant frequency and approximate closer a uniform current density on the structure.

The antenna return losses were measured with a HP8510 Vector Network Analyzer, which has the capability to measure the antennas' frequency response up to 26.5 GHz.

4.2.1 Procedure

First, the antenna layout was imported into the computer controlling the LPFK 95s/II milling machine. Then, the probe feed was soldered in the GF-B reflow oven. It is very important to do this step before integrating the switch since there's heat involved. The temperature of the reflow oven doesn't reach temperatures that will permanently damage the RF MEMS switches, but risks shall be avoided when possible. Later, the switches need to be integrated. The switches were held in place by using conductive epoxy as the adhesive material. Finally, the switches were connected to the structure by using the KS 4123 wire bonding machine.

The measurements of the resonance frequency at the different states of the switches were obtained from the HP8510 vector network analyzer. The characterization of the antenna was performed at the Radio and Scattering Compact Antenna Laboratory. The data was collected and plotted in Advance Design System (ADS) and AWR Microwave Office.

4.3 Simulation Software

The use of simulation software is essential in order to achieve our goals. The software used should facilitate the calculation of the location of the antenna's feed point, as well as the theoretical behavior of such structure. The program LineCalc by Advanced Design System was used in the design of a microstrip feed line, which was later changed for a probe feeding technique. CST MICROWAVE STUDIO ® was used to obtain preliminary design dimensions

and to simulate all the antenna structures in order to obtain the output responses. CST MICROWAVE STUDIO® (CST MWS) is a tool used for the 3D EM simulation of high frequency components, used in mobile communication, wireless design, and increasingly in signal integrity.

A Matlab Program is in development to be able to extract the specific radiation pattern measurements for a specific cut-plane at a specific frequency to determine the antenna radiation characteristics in space. Previous attempts were done on CAD Feko. Nevertheless, time was critical in achieving results and its use was discontinued.

4.4 Proposed Antenna Designs

After reviewing several papers, there's a myriad of antenna designs made in many different materials and with countless geometries. Several designs seem feasible. A novel antenna design could breed from designing a reconfigurable microstrip patch antennas since there's no previous work done with off-the-shelf components, to the best of my knowledge. First, the preliminary dimensions for the antenna patch were simulated in CST Studio®. Second, the feed location was swept across the structure to find the location at which the input impedance (Z_0) is 50Ω , in order to obtain its optimum dimensions. Once a model is achieved, the parasitic patches were integrated to study the coupling effects. Upon integrating the RF MEMS switches onto the structure, a goal-model was generated for the desired structure output responses. Finally, a prototype was fabricated for validation purposes.

The proposed antenna design consists of a reconfigurable single patch with extensions to the frequency driving parameter (length). Some other geometries, might also be studied to check for feasibility of using RF MEMS switches in reconfigurable antennas.

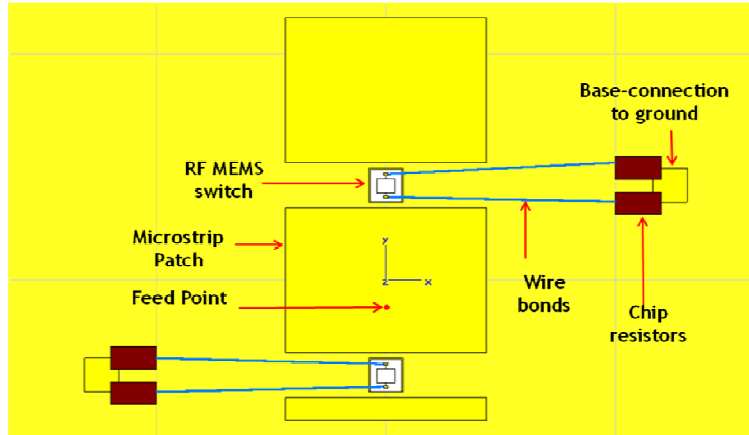


Figure 4.2 Proposed layout for the reconfigurable microstrip patch antenna.

4.4.1 Reconfigurable Microstrip Patch Antenna

First, the appropriate substrate for the design was selected, meaning the relative permittivity, desired thickness, and desired frequency of operation. Once selected, the step to follow is calculating the patch dimensions along with the substrate effects. This step determines the actual dimensions of the main antenna structure (width and length).

4.4.1.1 Theoretical Design of the Main Patch

The three essential parameters for the design of a rectangular Microstrip Patch Antenna are:

- Frequency of operation (f_r): The resonant frequency of the antenna must be selected appropriately. The design target is to have an antenna using the X-band at 10 GHz, reconfiguring to a different frequency band. The resonant frequency selected for the design is 10 GHz.

- Dielectric constant of the substrate (ϵ_r): The dielectric material selected for this design is Rogers Thermoset Microwave Material TM (TMM-4), double sided (for mechanical support) which has a dielectric constant of 4.5.
- Height of dielectric substrate (h): For the microstrip patch antenna to be used in possible satellite applications in needs to occupy a small volume. Therefore, a trade-off was made between size and a higher Q-factor on the patch. The height of the dielectric substrate is selected as 0.508mm (20 mils). If required, a thicker substrate will be considered.

For an efficient radiator, a practical width that leads to good radiation efficiencies is [10]:

$$W = \frac{1}{2f_r \sqrt{\mu_0 \epsilon_0}} \sqrt{\frac{2}{\epsilon_r + 1}} = \frac{c}{2f_r} \sqrt{\frac{2}{\epsilon_r + 1}} \quad (4-1)$$

where c is the free space velocity of light.

The effective dielectric constant of the microstrip antenna is calculated using Equation 2-6. Once the W and the ϵ_{eff} (for low frequency and $W/h \geq 1$) are calculated, the extension of the length (ΔL) is calculated using Equation 2-4. The actual length of the patch can now be calculated using Equation 4-2:

$$L = \frac{1}{2f_r \sqrt{\epsilon_{eff}} \sqrt{\mu_0 \epsilon_0}} - 2\Delta L = L_{eff} - 2\Delta L \quad (4-2)$$

Then, it is imperative to realize that for this type of antenna the frequency driving parameter is the length. Therefore, the antenna length dimension will be increased by using the RF MEMS switches. The feed point location is critical in determining the antenna's input impedance. The mutual coupling also causes a shift in input impedance, which is a behavior we

are relying on the shift the frequency of operation. Since the antenna is very small, the welding of the probe feed is expected to radiate and affect the performance of the patch. The frequency of operation of the extended structure will be approximated with the same equations used to calculate the length and width of any microstrip patch antenna.

4.4.1.2 Coupled Microstrip Patches

A technique used to change radiation patterns independently from frequency behavior is the use of electrically tuned or switched parasitic elements. The patches will be simulated as close as physically possible. All fabrication constraints must be considered when designing the interelement spacing of the patches. The switches are expected to change the coupling between the parasitic elements and the driven element, resulting in effective array behavior from a single feed point. Therefore, changes in radiation patterns are expected by changing the effective source currents on both the driven and parasitic elements.

4.4.1.3 Design of Patch Extensions, Hypothesis and Constraints

The first approach will be to change the operating frequency of the antenna by forcing the coupling between the main patch and neighboring patches. The main patch of the antenna was designed to operate at 10 GHz. The hypothesis for this approach is that the antenna will have a component of the radiating field causing a low coupling of the closely spaced parasitic elements, resulting in effective array behavior from a single feed point. One patch will have identical dimensions as the main patch, but the other will have a different length. The self similar structures should resonate at the same frequency, but the patch with different dimensions should resonate at a different frequency band. Since this patch has smaller dimensions it should resonate

at higher frequencies or accentuate a higher order mode by the change in input impedance over frequency.

There are physical constraints that need to be considered. One is the size of the switch. The footprints of the switches in question are 1.37mm x 1.42mm. The milling machine has a limitation on the path of metal it can remove from the surface layer of the substrate. The smallest drill bit is 0.250mm, which has to be taken into consideration when designing the spacing between patches. Also, since the patch is small, it is expected that the soldering of the probe feed might interfere with locating the exact point at which the input impedance is 50Ω .

4.4.2 Additional Reconfigurable Antenna Designs

Some possible additional designs have been considered in order to reconfigure the radiation pattern. The spiral antenna and dipoles have been analyzed and considered. These antenna geometries seem more suitable for this task. There's plenty of information on the geometries and some previous attempts have been published.

4.4.2.1 Spiral Antenna

Another technique used by researchers is using the linkage to their advantage, exploiting particular modes of operation to meet specific system requirements. Antennas with multiple resonant modes often exhibit very different radiation characteristics for each of the modes. Careful design can allow the bands to be switched or used simultaneously. The antenna's innate properties can be exploited without struggling to suppress or eliminate the frequency response. One such example of this approach can be found in [62], where the multiband properties of slot spiral antennas can be used to achieve different radiation patterns over different frequency bands.

These antennas were intended for use in communication in different wireless systems. Figure 4.3 presents the possible antenna structure for the spiral antenna, with strategically placed switch pads.

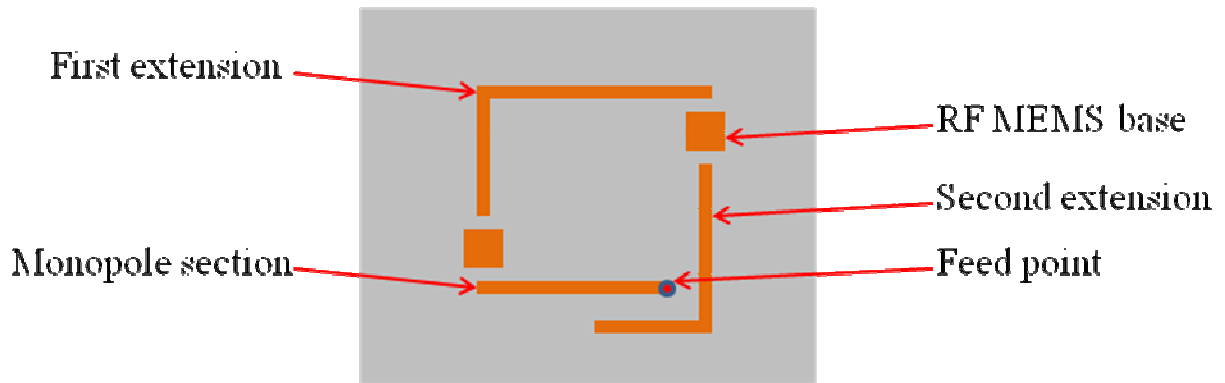


Figure 4.3 Proposed reconfigurable single-arm square spiral antenna.

4.5 Chapter Conclusions

In this chapter the materials and methodology used to accomplish the research were described. The proposed antenna structures were presented, along with the design process, simulation software and prototype fabrication. The measurements are presented in the following chapter. The results will be presented, analyzed and explained.

Chapter 5

Results and Discussions

5.1 Proof of Concept

The preliminary dimensions for the antenna structure were obtained from Dr. Dimitrios E. Anagnostou. The purpose of this experiment was to fabricate and characterize the antenna system, and to compare it against simulation results. This part will prove that the RF MEMS switches taken off-the-shelf can be integrated into an antenna structure and provide frequency reconfigurability. Other issues will be studied, to include ease of assembly, integration of electronic elements and multiuse of the resulting system.

5.1.1 Antenna System

The antenna studied herein is a folded loop monopole antenna designed to operate at a higher-order mode in order to produce directive patterns in the 14 GHz to 16 GHz range with a return loss better than -10dB. The two ohmic contact cantilever Radant RF MEMS switches were integrated in the antenna by using a wire bonder. These switches were selected because of their low power consumption, long life cycle, and RF performance [63]. The switches were introduced to allow the extension of the “simple monopole” geometry into a “folded monopole” operating at higher frequencies. It is also expected to reconfigure the radiation pattern. Further measurements must be done in order to demonstrate this concept. The antenna layout and the antenna structure after assembly are shown in Figure 5.1 (a) and (b).

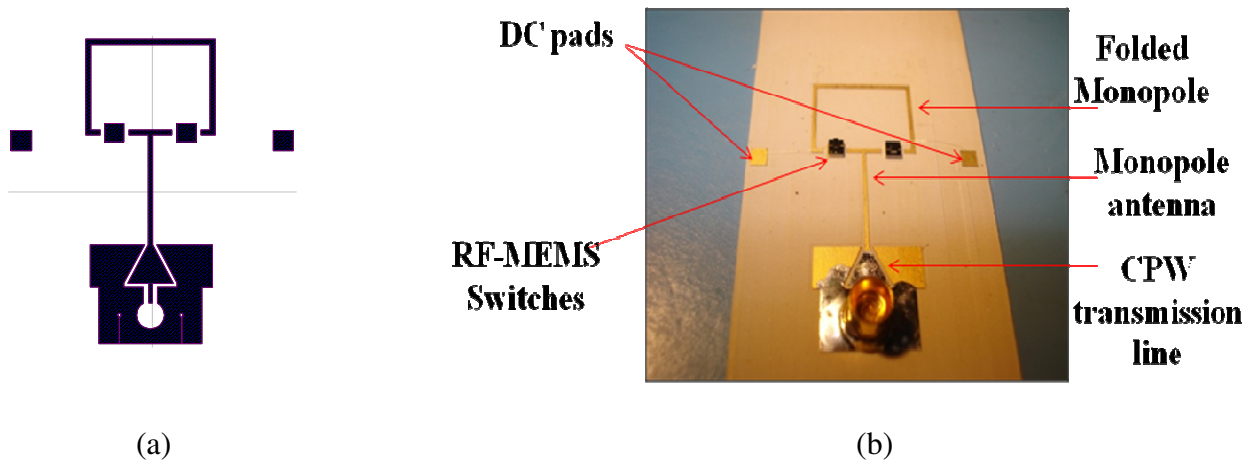


Figure 5.1 Monopole-folded monopole (a) layout and (b) photograph after assembly.

5.1.2 Problems Encountered and Lessons Learned

Some of the problems encountered are listed herein:

- The substrate is too brittle.
- Extra welding was needed to support probe feed.
- It is very difficult to replace the switches if damaged.
- Switches have isolation problems, and failed to perform appropriately.
- The wire cannot be solder on copper surface because of oxidation.
- The 0.7 mil wire doesn't provide good adhesion to structure.

The integration of the monopole-folded monopole antenna faced several problems that were not that trivial. Trade off is needed between performance and mechanical support, specifically when dealing with the bandwidth. The antenna couldn't stand any hits or mishandling since the substrate was ceramic and only 15 mils thick. For future designs, a microstrip substrate with bottom ground plane layer will be used with a thicker substrate to avoid

having a high Q factor. The surface mount probe feed also presented difficulties since it kept detaching from the antenna when trying to measure resonance frequency or radiation patterns. The probe feed had a full detent, and it was slightly hard to remove the antenna from the characterization set up without exerting too much force to the antenna. Extra welding was used to hold the probe feed in place with the possibility that it may radiate, cause diffraction of the energy, or affect the antenna performance in general. For future designs, a probe feed will be integrated from the bottom of the patch to avoid any interference with the radiation pattern in broadside.

The implementation of the switches faced some changes as well. The switches cannot be attached with epoxy, if they need to be replaced. However, a conductive adhesive is needed in order to have the switch ground connected to the base plate underneath. Also, the base plate needs to be connected to the ground. A drill hole was included in every patch serving as a base plate for the switches to later create the vias with an electroplating technique. This will provide a positive connection between the switch ground plane and the antenna ground. This interconnection should fix the floating ground of the switch that presented isolation problems.

Besides isolation problems, the switches presented a reliability problem. The reason they failed was because they are sensitive to electro-static discharge (ESD) events. Also, a circuit for safe discharge dissipation of the dc power is required and safe apparel for handling them. Later versions of this switch (RMSW 200 and 201) are better protected against this hindrance.

The gold wires used for wire bonding were unable to positively solder to the copper surface because of oxidation, even after cleansing. Gold to gold contact is essential in this task since it is more resistant than copper to oxidation. However, a thin diffusion barrier is required

between copper and gold since they interact too easily. Nickel (Ni) is normally used as a diffusion barrier. Because of the diameter of the wires, they were difficult to handle and were not providing good soldering to the structure. They were later replaced by 1.5 mils thick gold wires. The wire bonding effect on the antenna performance will be minimized by using the least amount possible for the switches integration.

5.1.3 Results and Discussions

All four configurations of the monopole antenna were studied. The return loss was the main parameter used to analyze and determine the resonant frequency. The resulting operating frequency bands are summarized in Table 5.2. In the ‘Off-Off’ configuration a well-matched band from 14 GHz to 15.79 GHz with better than -10 dB return loss was achieved. The measured and simulated results after de-embedding for the feed line extension matched well and are shown superimposed in Figure 5.2. The simulated antenna pattern shows good pattern stability from 14-16 GHz, as shown in Figure 5.3.

Configuration and Name		Operating Frequency
Off-Off	Monopole antenna	14-15.79 GHz
Off-On	Half loop spiral antenna	9.61-10.43 and 12.41-18.08 GHz
On-Off	Half loop spiral antenna	9.93-10.63 and 12.41-18GHz
On-On	Folded monopole antenna	15.76-17.22 GHz

Table 5.1 Operating frequency bands for the configurations of monopole-loop antenna.

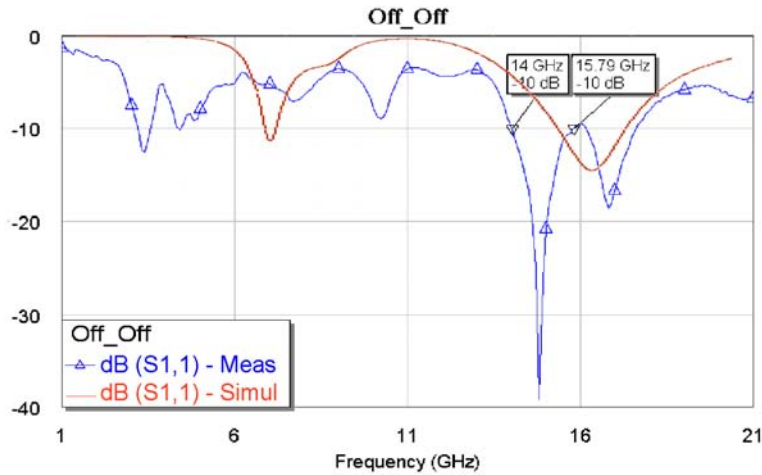


Figure 5.2. Return loss of the monopole-folded monopole in the Off-Off switch configuration.

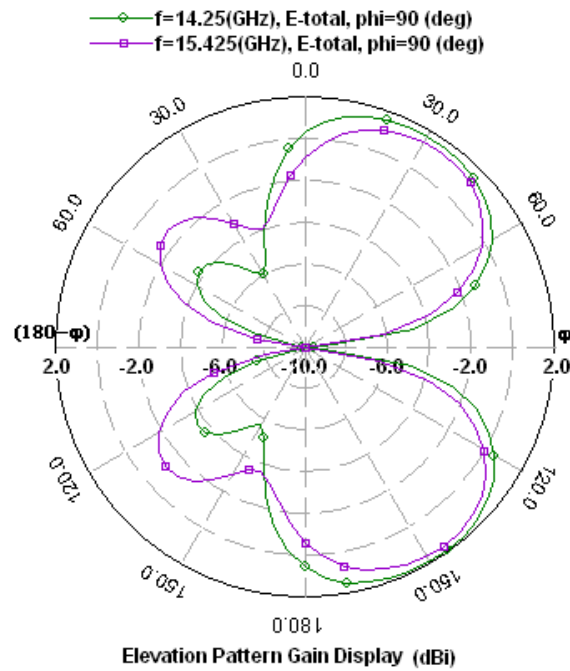


Figure 5.3 Simulated radiation patterns at 14.25 and 15.425 GHz.

For the ‘On-On’ configuration, the antenna’s operating frequency band reduces its first resonance to 4.25GHz. However due to the MEMS wire bonding (most likely) this resonance was not observed in the measurements. Instead, its operating frequency ranged from 15.76 GHz to 17.22 GHz, as shown in Figure 5.4. The simulated radiation patterns of the monopole

configuration from 13 GHz to 17 GHz are presented in Figure 5.5. It presents a tendency to null the radiation at 90° and 180° due to the loop parasitic element of the antenna located at these angles in the azimuth plane. The antenna demonstrated reconfiguration in a continuous band, increasing the operating frequency band. This reconfiguration can be better observed if both measurements are placed into the same graph (see Figure 5.6). The measurements are fairly similar to the predicted behavior.

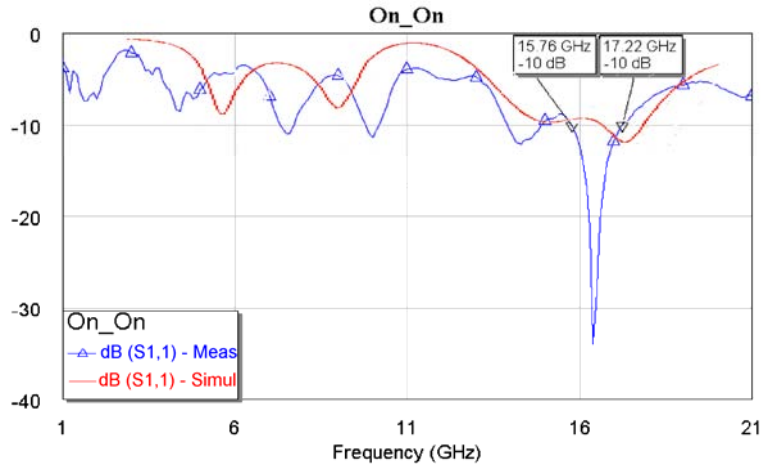


Figure 5.4 Return loss of the monopole-folded monopole in the On-On switch configuration.

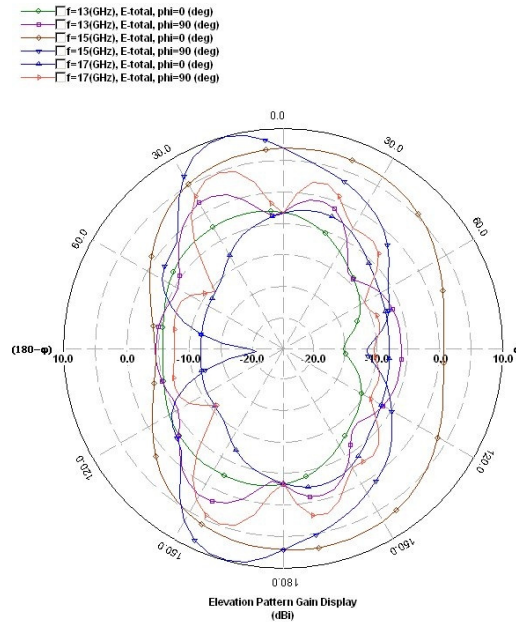


Figure 5.5 Simulated radiation patterns of monopole-loop at 13 GHz, 15 GHz and 17 GHz.

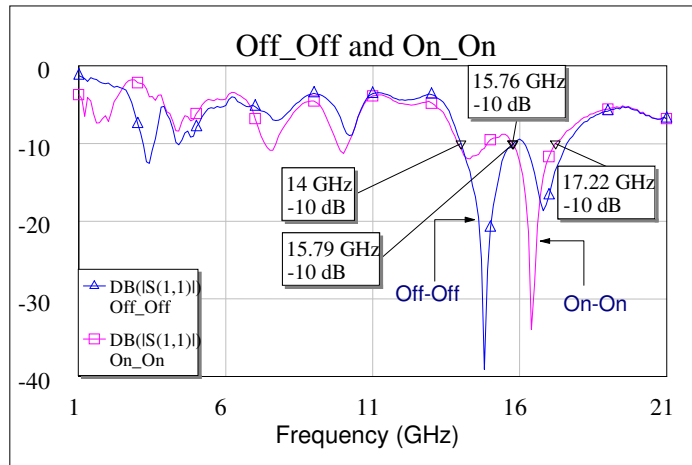


Figure 5.6 Return loss of the Off-Off and On-On states of the switches combined.

The other two states ('Off-On' and 'On-Off') were also measured and, as expected, were very similar in behavior due to the symmetry of the antenna. An open circuit was created in the switch that was not of interest during measurements since the signal was fed to both switches through the feed line. The return loss measurements for both configurations are presented in Figure 5.7. Gain and radiation patterns are shown in Figure 5.8, 5.9, and 5.10. They present the antenna behavior in the operating frequency band.

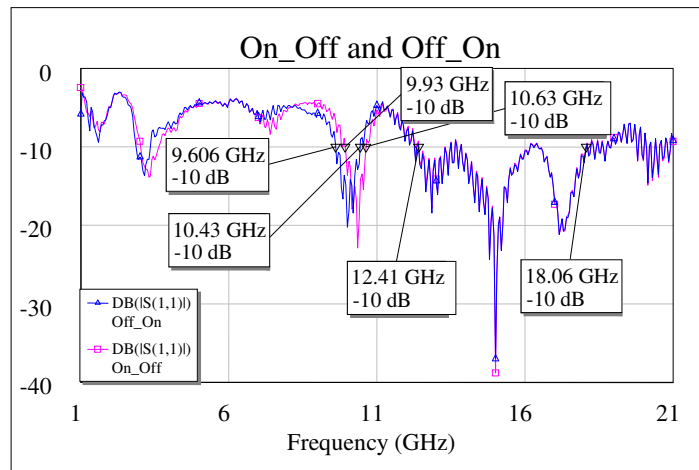


Figure 5.7 Return loss of the Off-On and On-Off states of the switches.

After observing the return loss for these configurations, a periodic ripple was noticed. The graph smooth out after placing some absorber right over the switch that was turned off, coming to a conclusion that the ripple is caused by mutual coupling between the monopole and the folded-monopole section.

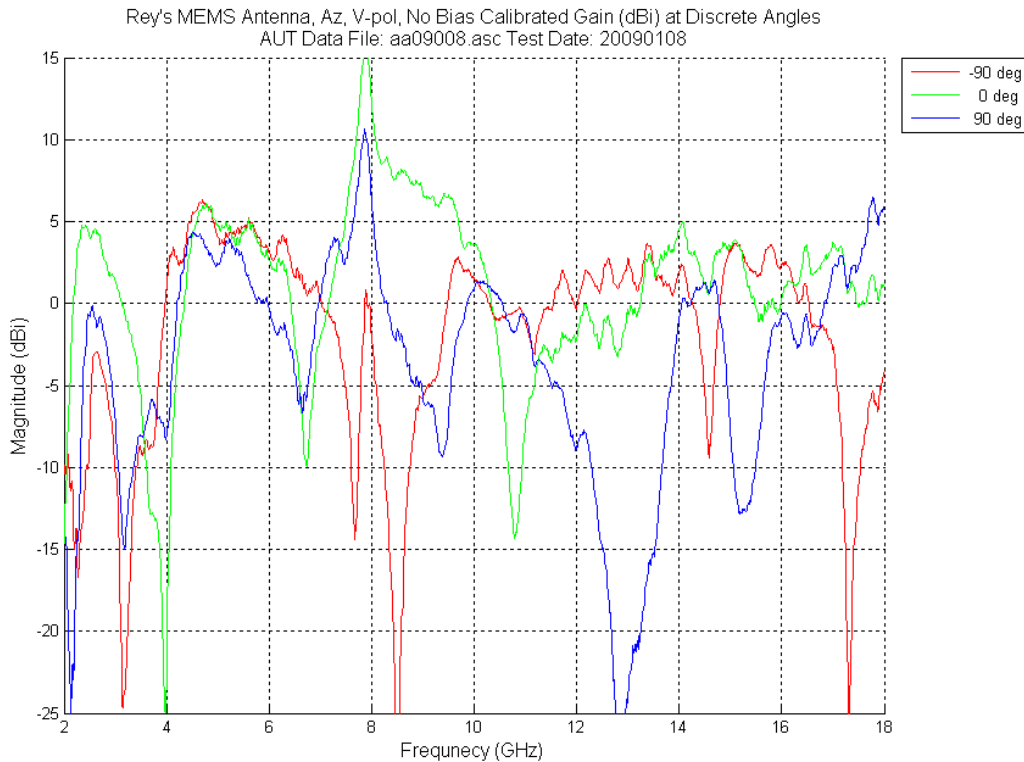


Figure 5.8 Gain vs frequency of the monopole-loop before actuating the switches.

In Figure 5.8 the highest gains seem to be at 8 GHz at 0 degrees in the azimuth plane cut. Nevertheless, the radiation efficiency needs to be studied in order to better understand the antenna performance at this frequency. A 5dB gain is observed at the resonance frequency, starting at 14 GHz.

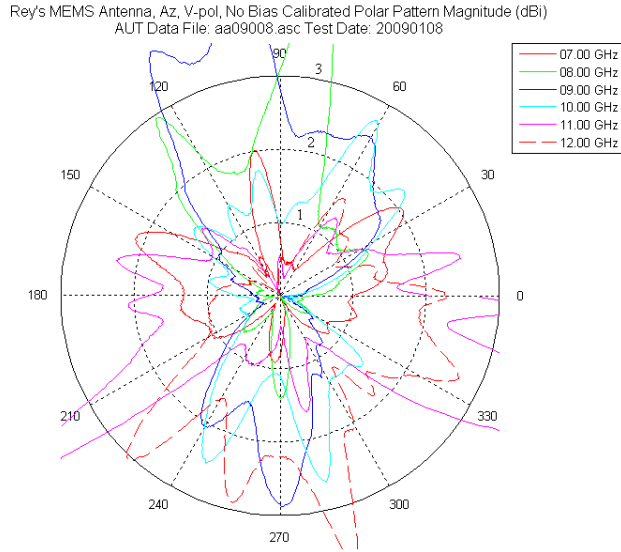


Figure 5.9 Radiation pattern from 7-12 GHz in azimuth cut.

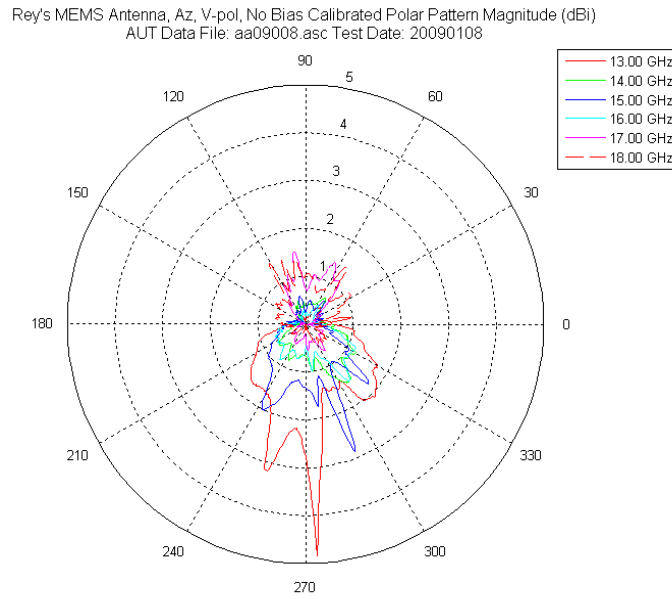


Figure 5.10 Radiation pattern from 13-18 GHz in azimuth cut.

Disclaimer: The Matlab code used to extract this data is proprietary of the Air Force Research Laboratory, and cannot be published.

5.1.4 Conclusion of the Proof of Concept

The reconfigurable monopole to folded-monopole design presented herein was fabricated and characterized. A multi-frequency antenna was proved possible by actuating off-the-shelf RF-MEMS switches integrated in the antenna design. There are some difficulties actuating both switches separately with hot switching. Future integration of a control system will solve this problem, but separate dc-bias lines will be needed. Some lessons learned in the RF-MEMS switch integration process are that the actuation voltage of both switches should be around the same magnitude, since the switches can be damaged if not carefully actuated, and a protective circuitry is required to provide a dc-current path to ground. It is proven that lump RF MEMS switches can be used to reconfigure an antenna structure, and consequently its operating frequency band.

5.2 Switch Characterization

MEMS switches have introduced new approaches to reconfigurable antenna designs. Their low power consumption and high linearity have made them popular in such applications. They have proven to be reliable if design process and packaging are done appropriately. The switch characterized herein was tested for insertion loss and isolation measurements.

The main goal is to prove that the RF MEMS switches have a good response in terms of isolation, insertion loss, and linearity. A switch model shall be created for possible integration in future designs. The inherent low power consumption makes them attractive for many low and medium power applications. A better prediction of behavior could be achieved if the model could be integrated into the antenna simulations.

5.2.1 Operational Principle

The operating frequency of the antenna is electrostatically tuned by applying a dc bias voltage between the patch and the ground plane. If the signal is fed through the feed line, the switching action will be called “hot switching” since the drain and source terminals will be at different potentials. To do “cold switching” the bias voltage must be applied to the pull down electrode, also called “gate”. By doing so, the measurement of radiation patterns will be limited due to the proximity of the dc probe station to the aperture. A hot switching technique will be used to actuate the switches. Upon actuation, the movable ohmic contact cantilever of the RF MEMS switch deflects downward toward the fixed ground plane due to electrostatic force of attraction caused by the applied dc bias voltage on the pull down electrode (ranging from 80 V to 90 V-dc). This deflection allows for the integration of segments to the main antenna, resulting in an increase in coupling between the patches. This effect produces a shift in the input impedance, thus causing a shift in resonant frequency. The switching speed was not measured, but it should range, per the manufacturer, around 10 μ s to turn on and 2 μ s to turn off [62].

5.2.2 Switch Characterization System

The switch was characterized using a network analyzer, a dc-probe station, and an amplifier system put together to provide the required high voltage-low power requirements. The layout for this system is shown in Figure 5.11. The oscilloscope was used to ensure the actuation voltage was calibrated accurately since the setting for the amplifier was a calibrated knob.

After mounting the RF MEMS switch onto a metal plate to serve as ground plane, it was connected to two coplanar waveguide (CPW) transmission lines by wire bonding two 0.7 mils

thick wires as shown in Figure 5.12. The CPW transmission line will be the contact point of the ground-signal-ground probes used in RF measurements. The system was then placed on a dc-probe station to do an S-parameter measurement. A system was developed to measure the cold switching response of the switch, which means that the source and drain are at the same potential when the switch opens and closes. This will ensure that no additional energy dissipates at the contacts during the switching events.

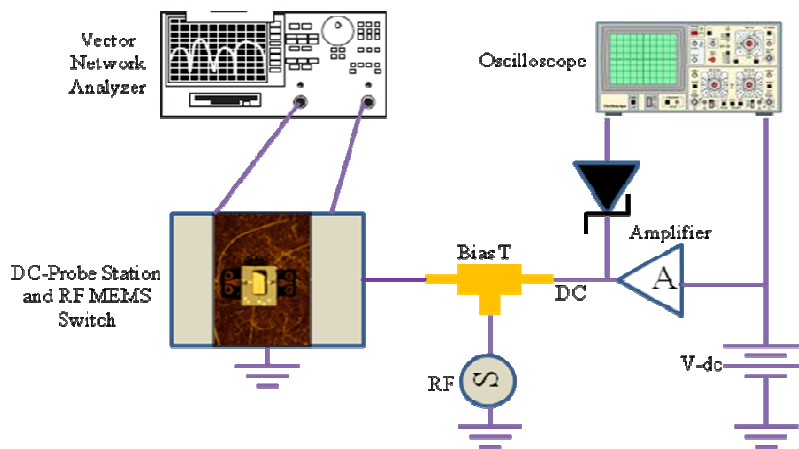


Figure 5.11 System used for switch characterization.

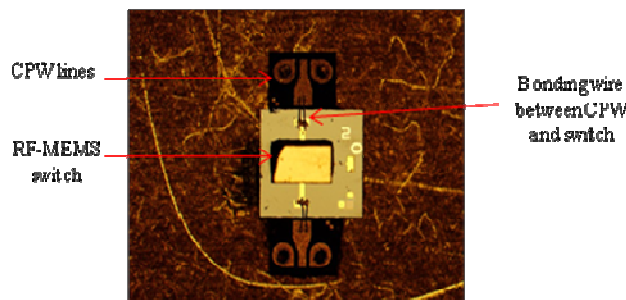


Figure 5.12 Test configuration for Radant-RF MEMS switch with microstrip to CPW adapters used for switch characterization.

5.2.3 Results and Discussions

One of the parameters measured was the return loss of the switch when actuated with different voltages. It first actuated at 72V-dc. Then the voltage was increase up to 80V-dc and 90 V-dc. The results proved that the switch can not only withstand the high dc-voltage, but also it has a better response in that region. The S11 was below -15 dB in the operating frequency band and the insertion loss(see Figure 5.13). The results were similar to the performance described by the manufacturer up to 20 GHz.

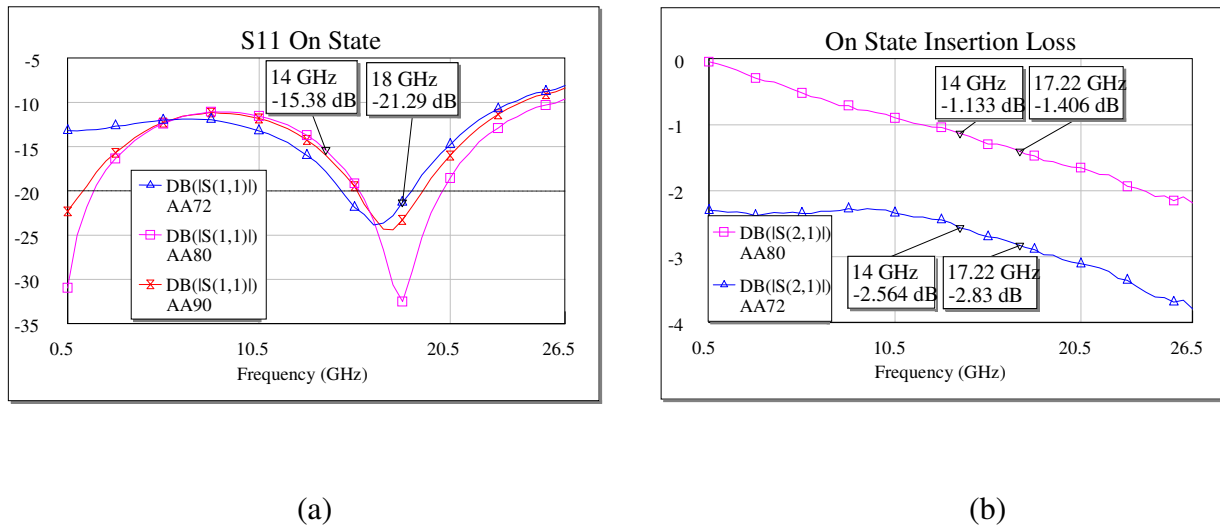


Figure 5.13 (a) Return loss and (b) insertion loss vs frequency under different actuation voltages.

A model was created for the switch (see Figure 5.14). The switch model was compared against the switch behavior for a future implementation in the antenna simulations. The model resembles the switch behavior for return loss in the “Off” state and “On” state (Figure 5.15 and 5.18) in the operating frequency region.

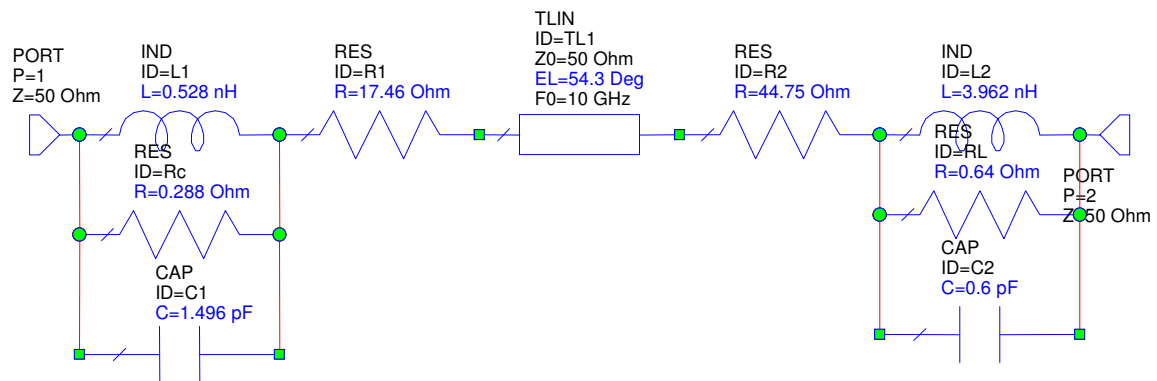


Figure 5.14 Switch model for RMSW101 version.

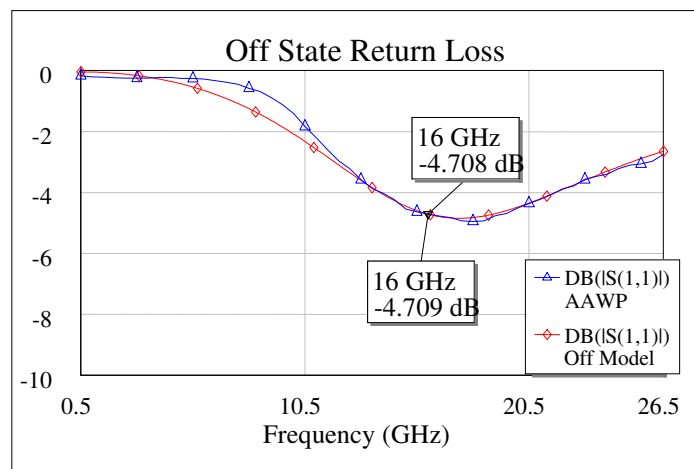


Figure 5.15 Return loss of the Off-Model compared to the measured return loss of the switch.

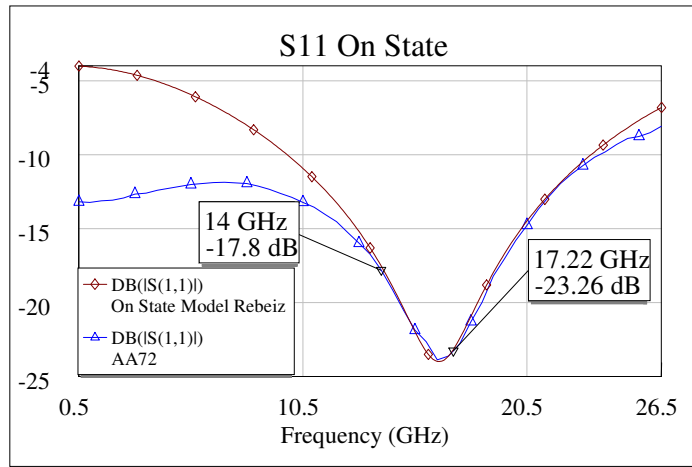


Figure 5.16 Return loss of the On-Model compared to the measured return loss of the switch.

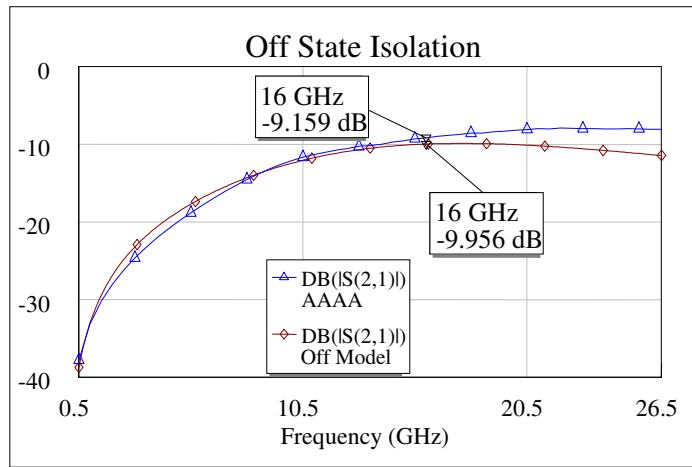


Figure 5.17 Isolation of the switch compared to the switch model.

Another parameter that was studied was the isolation of the switch when in the “Off” state. It showed isolation below -8.78 for the operating frequency band. When compared with the data sheet, it is close to the predicted behavior. Later versions of the switch show an improvement in this characteristic. The isolation (Figure 5.17) and the isolation phase behavior were compared to the switch model as well (Figure 5.18).

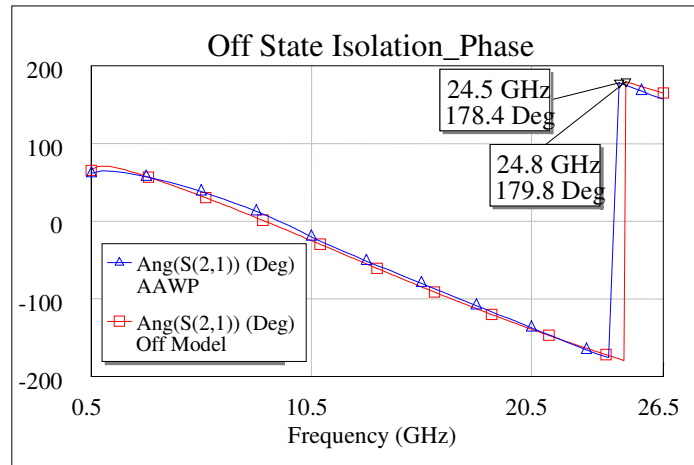


Figure 5.18 Isolation phase of the switch compared to the switch model.

The switch model consisted of an equivalent circuit that resembles the behavior of the switch in performance. It was developed using lumped components between two ports in AWR Microwave Office 2007. This model was generated following the same configuration that other researchers have done for their particular device response [64].

Several testing precautions were required when handling the RF MEMS switches. They have been fabricated without any electrostatic discharge protection. In addition to this fact, their extremely small size, low on-resistance, and minimal parasitic capacitance, makes the switches sensitive to transients which may arise from handling and test system cabling. The stored charge may inadvertently conduct through the switches, resulting in immediate permanent damage to the devices. All instrumentation must share the same chassis ground, since a difference in potential between grounds can cause the device to suffer an ESD event.

In general, the frequency response of the switch met the requirements for the reconfigurable antenna design, with an insertion loss less than 0.5 dB and return loss greater than 18dB across the operating band.

5.2.4 Integration with the Antenna

The RF MEMS switches were integrated onto the antenna platform using wire bonding, having the wires as the RF path between the switch and the antenna. The reliability of the switches is tied to their proper handling. There are some important aspects about the switches that need to be considered, such as failure mechanisms and electrostatic discharge (ESD).

The failure mechanisms of the dc-contact switches are due to damage, pitting, and hardening of the metal contact area. These effects need to be addressed by the manufacturer during design. ESD occurs when two objects at different potentials come into direct contact with each other, or when their proximity causes the polarization of the air molecules between the two objects. This is one of the major issues and cause of failure in semiconductor industry. The minimization of movements in the work area, as well as the use of ESD-safe apparel (discharge wrist bracelet) will help in minimizing static charges generated by personnel. After contacting the manufacturer, a protection circuit was required to protect the device and to provide safe dissipation of the charge build-up. Later versions of the switch were design to protect for these events.

Figure 5.19 shows a picture of the RF MEMS switch used, and the recommended circuit for ESD protection.



Figure 5.19 (a) RF-MEMS switch used in the antenna subsystem and (b) the protection circuit recommended for safe dissipation of the charge build-up [65].

The manufacturer recommended the circuitry in Figure 5.19 (b) for the integration of the RF MEMS switch to any platform. Two ground return resistors are required to protect against parasitic capacitances in the test system that will cause capacitive coupling of the actuation signal to the drain and source terminals. In order to minimize hot-switching caused by the coupled signals (this reduces the life span of the devices) the test system must provide a path (resistance 40-100 K Ω was recommended) from the drain and source terminals to dc-ground. This was not done previously and the switches were not responding as expected due to incompleteness of the dc-path. The resistors could be replaced with inductors.

The reliability of RF MEMS switches is of concern for long term applications. There are many researchers working on this effort. The reliability of the dc-contact switches is strongly related to the metal contact used, therefore the use of gold. All implementations should be carefully analyzed to protect the switches against the most critical problem: ESD events. The mechanical failure of the switches used in this thesis was not a big concern, since the deflection is approximately 1-4 μm (less than 5% of the cantilever's thickness, ranging from 75-350 μm).

The antenna layout had to be modified slightly in order to integrate the RF MEMS switch. A patch for the placement of the switch shown in Figure 2(a) was needed. This was done with a via hole, and the patch was connected to the ground plane. This will avoid having a floating ground on the switch, which will cause isolation problems. A via hole was made from the patch which served as switch base plate through the substrate up to the ground plane. Also, another patch was needed for the integration of the protection circuit for safe static charge build-up dissipation (shown in Figure 2(b)). The via-holes were connected using electroplating, thoroughly protecting the rest of the structure.

The final antenna system for the proof of concept with all components integrated is presented in Figure 5.20 as the radiation pattern was being measured for the azimuth plane.

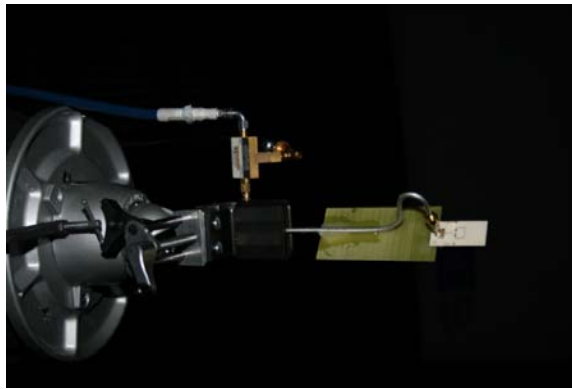


Figure 5.20 Measurement of radiation pattern for azimuth angle.

5.3 Reconfigurable Microstrip Patch Antenna Design

Now that the concept has been proven, a design procedure will be outlined which should lead to a practical design of a rectangular microstrip patch antenna. This procedure follows the selection of material to work with, including the dielectric constant of the material (ϵ_r), the resonant frequency (f_r), and the height of the substrate (h).

For circular polarization a single patch can be excited using two feeds, with one feed delayed by 90° with respect to the other. This drives each transverse mode TM_{10} and TM_{01} with equal amplitudes and 90° out of phase. Each mode radiates separately and combines to produce circular polarization. The most common approach is to use a single feed and a 90° hybrid coupler to produce a maximized current flow leading the vertical radiated electrical field. A quarter-cycle later, the situation will have reversed and the field will be horizontal. The radiated field will thus rotate in time, producing a circularly polarized wave [66].

For a single linearly polarized antenna the calculations are much simpler. This design is described as linearly polarized since the electric field only varies in one direction. This

polarization can be either vertical or horizontal depending on the orientation of the patch. All the calculations done for the antenna dimensions follow the selection of material to work with, to include the dielectric constant of the material (ϵ_r), the resonant frequency (f_r), and the height of the substrate (h). Table 1 summarizes the properties for the antenna design presented in this paper and Figure 1 shows its layout.

5.3.1 Design of Main Patch

Step 1: Selection of substrate and resonance frequency.

Material chosen: Rogers TMM® 4

Thickness $h = 20 \text{ mils} = 0.508\text{mm}$

Dielectric constant $\epsilon_r = 4.5$

Standard copper cladding $\frac{1}{2} \text{ oz. (17}\mu\text{m)}$, Ni barrier, Au thin film layer on top

Resonance frequency $f_r = 10 \text{ GHz}$

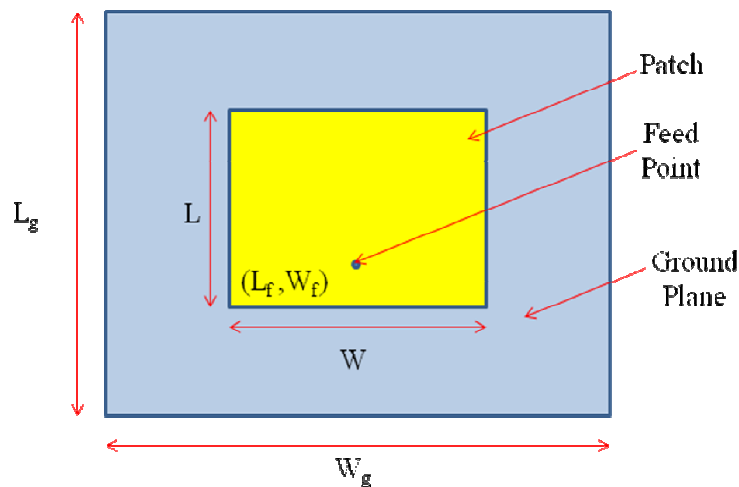


Figure 5.21 Top view of Main Patch.

The design equations for the rectangular microstrip patch are derived from the transmission line model, which is one of the most accurate for thin substrates [4], [10]. It represents the microstrip antenna by two slots, separated by a low impedance (Z_c) transmission line of length L .

Step 2: Calculation of the Width (W).

Once the substrate and resonance frequency have been identified, the width of the patch will be determined:

$$W = \frac{1}{2f_r \sqrt{\mu_0 \epsilon_0}} \sqrt{\frac{2}{\epsilon_r + 1}} = \frac{c}{2f_r} \sqrt{\frac{2}{\epsilon_r + 1}} = 9.045mm$$

Step 3: Calculation of Effective dielectric constant (ϵ_{r-eff}): The next equation gives the effective dielectric constant as:

$$\epsilon_{r-eff} = \frac{\epsilon_r + 1}{2} + \frac{\epsilon_r - 1}{2} \frac{1}{\sqrt{1 + 12 \frac{h}{W}}} = 4.1026$$

Step 4: Calculation of the Effective length (L_{eff}): The effective electrical length of the patch is:

$$L_{eff} = \frac{1}{2f_r \sqrt{\epsilon_{eff}} \sqrt{\mu_0 \epsilon_0}} = 7.406mm$$

Step 5: Calculation of the length extension (ΔL): The incremental length of the patch gives:

$$\Delta L = 0.412h \frac{(\epsilon_{eff} + 0.3) \left(\frac{W}{h} + 0.264 \right)}{(\epsilon_{eff} - 0.258) \left(\frac{W}{h} + 0.8 \right)} = 0.233mm$$

Step 6: Calculation of actual length of patch (L): The actual length of the antenna is:

$$L = L_{eff} - 2\Delta L = 7.406mm - 2*0.233mm = 6.940mm$$

Step 7: Calculation of the feed point location: The feed point location is approximately given by:

W_f = center on the patch

$$L_f \approx \frac{1}{6}L = 1.157mm$$

This parameter will be studied in the simulations to validate this approximation.

Step 8: Calculation of the ground plane dimensions (L_g and W_g): The transmission line model is applicable to infinite ground planes only. For practical applications, we need to have a finite ground plane. As a rule of thumb, the size of the ground plane is greater than the patch dimensions by approximately six times the substrate thickness all around the periphery. It's been proven that similar results for finite and infinite ground plane can be obtained following this approach. The ground plane dimensions would be given as:

$$L_g = 6 * h + L = 9.988mm$$

$$W_g = 6 * h + L = 12.093mm$$

5.3.2 Design of Patch Extensions

Now that the main patch has been designed, an identical patch was closely placed to this patch next to one of the radiating edges to allow for coupling. The patch with different dimensions was placed at the other radiating edge of the patch in an effort to obtain another operating band. The dimension of the identical patches was kept with length of 6.94 mm and width of 9.045 mm. The other patch was arbitrarily chosen to have the same length as the

spacing between the patches, 2mm.

From the simulations of the main patch alone, we obtain an electric field distribution as expected from a rectangular patch antenna (shown in section 5.3.3). The coupling between the side-by-side elements is a function of the relative alignment. The alignment used for the design of the antenna is referred to as E-plane alignment, since they are collinearly aligned along the propagating E-plane. E-plane alignment shows more coupling than the H-plane alignment, due to surface wave excitation (the lowest order or dominant surface wave mode is TM_{01} with zero cutoff frequency followed by TE_{10}) [67], [68]. For an edge to edge separation (s), the E-plane exhibits the smallest coupling isolation for $s < 0.10\lambda_0$, thus selecting for the interelement spacing a distance of less than 3mm for the design ($\lambda_0 = 3\text{mm}$ at 10 GHz).

The patches were coupled both vertically and horizontally in the simulations to justify the alignment in the E-plane. When coupled horizontally at the length point where the input impedance was 50Ω , the resulting impedance dropped, as if the patches behaved as four 50Ω resistances in parallel.

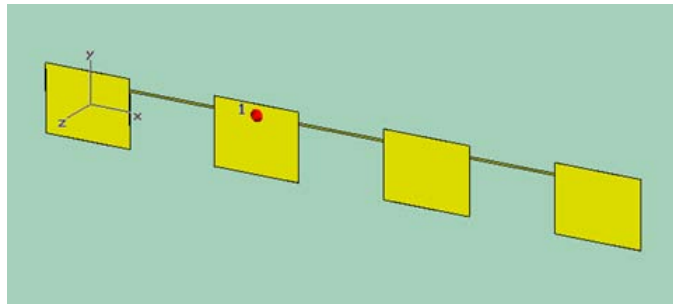


Figure 5.22 4 Patches in parallel simulated as hard wire modeling.

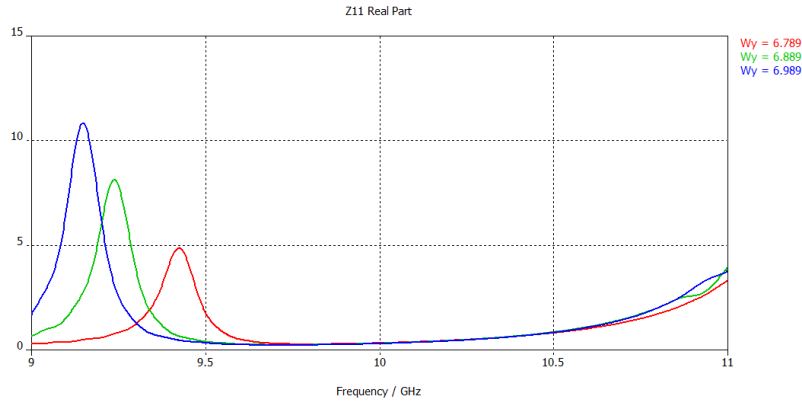


Figure 5.23 The real impedance of 4 patches in parallel.

Figure 5.22 shows the 4 coupled patches behaving as 4 parallel resistors, resulting in a maximum real impedance of approximately 12Ω (Figure 5.23). Therefore, this approach cannot be followed as it will only match the system impedance locating the point at which the input impedance is approximately 200Ω when actuating all switches, and 100Ω when actuating one switch.

The next experiment will show the reconfiguration of the patch length. It is important to notice that the parameter that drives the resonance frequency is the length. This observation resulted from multiple simulations showing the edges at the end of the length parameter as the radiating edges, shown in the next section.

5.3.3 Simulations and Results

The first step to verify that the antenna design is accurate is to simulate the dimensions calculated in sections 5.3.1. The main antenna patch was simulated by itself to find the point at which $Z_{in}=50\Omega$ and the dimension at which it will resonate at the desired frequency. The other patches were integrated into the simulations to study the coupling with the main patch. The

switches and protection circuit presented almost no effect on the resonance frequency. S12 parameter describes the coupling between neighboring radiating elements. The inter-element spacing was varied to see the effect on the coupling and excitation of surface waves. The minimum spacing between the elements was 2mm, leaving 1.5mm for the switch footprint since the minimum spacing that the drill bits can remove is 0.25mm.

The following figures show the results of the simulations of the main patch by itself. Later simulations will show the effect of the coupling of the antenna patch, along with the performance parameters that describe the antenna behavior. From the simulations of the main patch alone, we obtain the E-field intensity out of the radiating edges (Figure 5.22) and the electric field distribution as expected from a rectangular patch antenna (Figure 5.23).

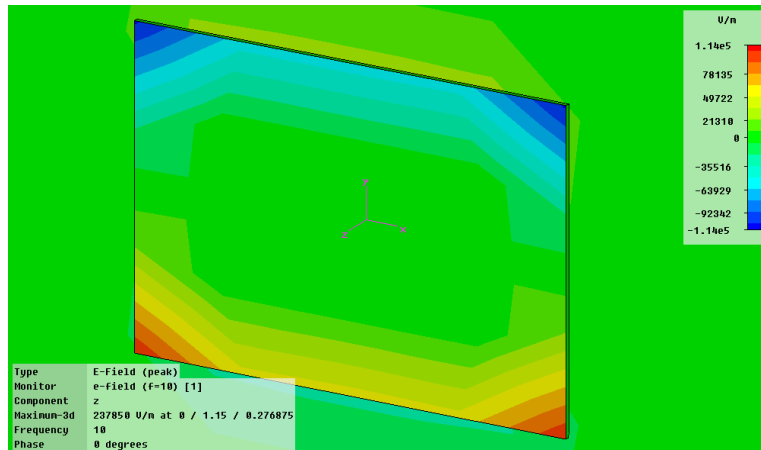


Figure 5.24 Microstrip patch showing the E-field intensity out of the radiating edges.

The E-field intensity is greater at the corners. The non-radiating edges show no radiation. These edges were designed to be 180° different in wavelength, therefore cancelling out their radiation. This should minimize the cross polarization. The E-field also shows that one edge is opposite in field polarity related to the other.

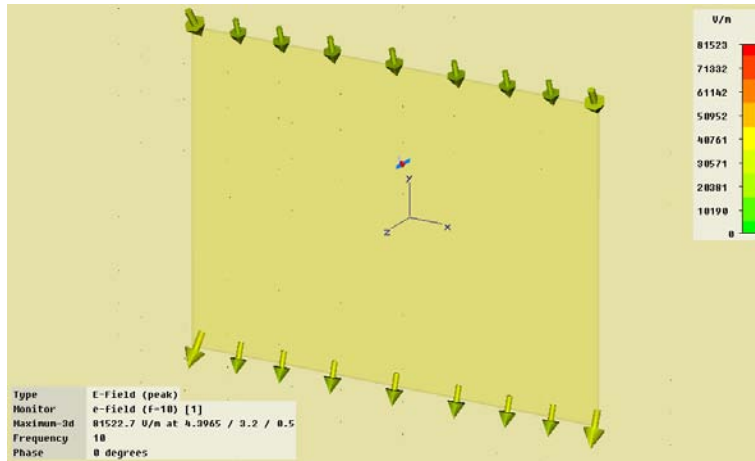


Figure 5.25 E-field lines entering and exiting the microstrip patch.

The return loss (S_{11}) for the main patch alone is presented in Figure 5.24 (a) and (b), shows the return loss of the patch resonating at 10 GHz as designed, in rectangular and Smith Chart plots, respectively. The bandwidth obtain is between 9.84 GHz and 10.16 GHz with better than -10 dB return loss, and a center frequency in 10 GHz. The inherent narrow bandwidth of the microstrip patch is immediately noticed. Some antenna designers have presented patch antennas with “chamfering” or cutting of the corners in order to create broadband designs. But this approach increases the resonant frequency of the antenna. This experiment was run and proven truth.

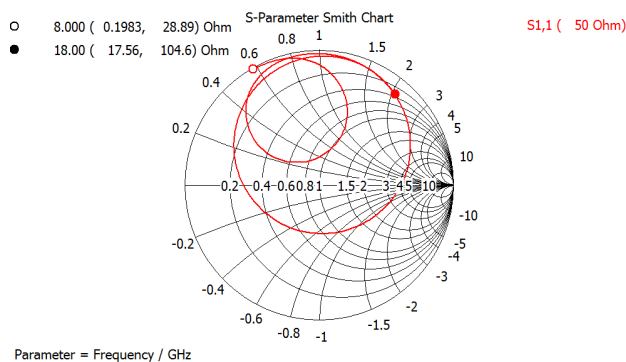


Figure 5.26 (a) S_{11} plotted in a Smith Chart from 8-18 GHz.

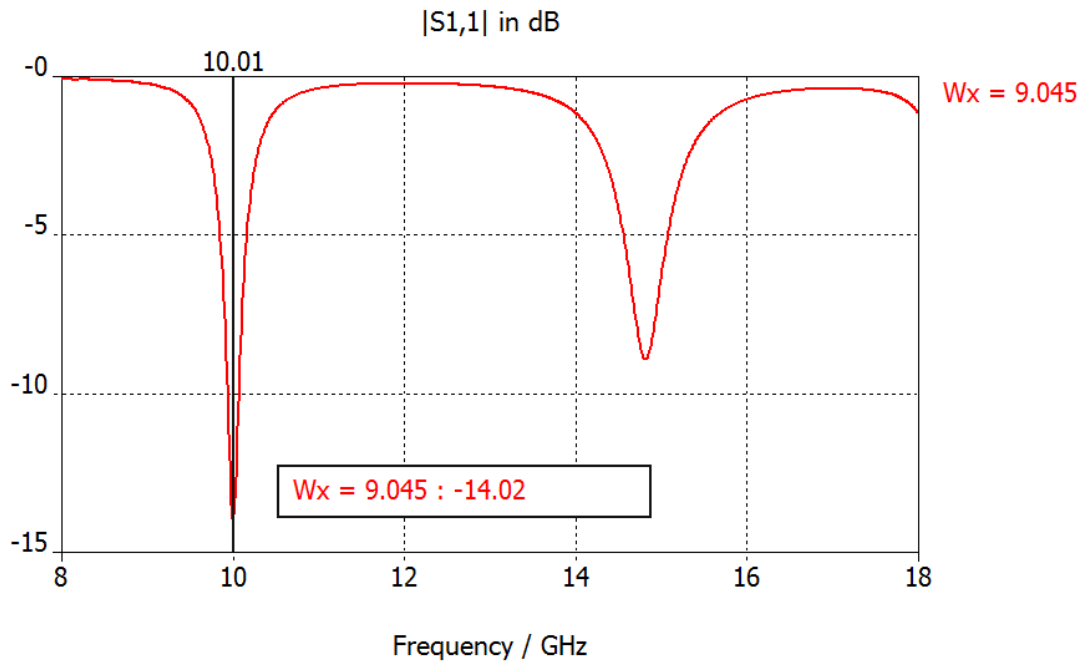
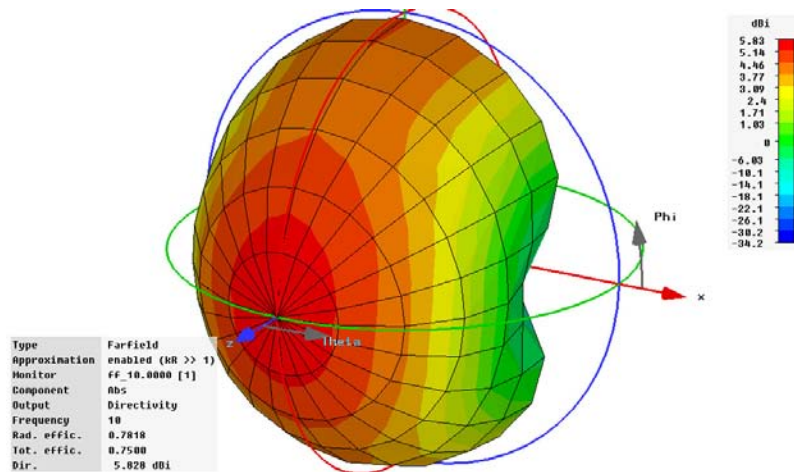
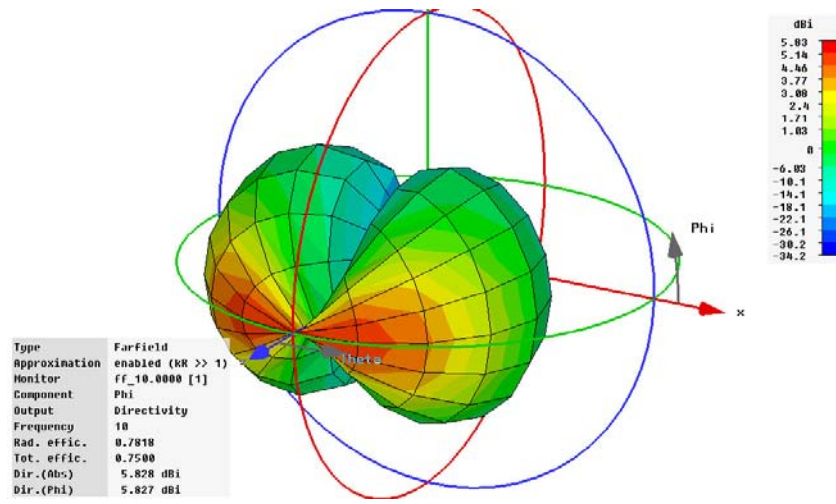


Figure 5.26 (b) S11 dB-parameter shows resonance at 10 GHz.

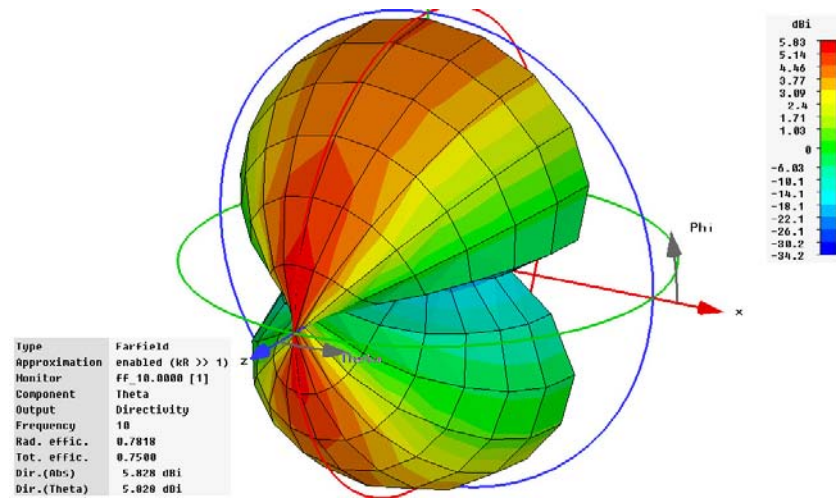
Figure 5.27 shows the expected radiation pattern at different plane cuts for a microstrip patch antenna, assuming an infinite ground plane, with a gain of 5.8 dBi in broadside or theta plane and a radiation efficiency of 77% at 10 GHz.



(a)



(b)



(c)

Figure 5.27 Expected radiation pattern of the microstrip patch without actuation of switches at 10 GHz (a), then in phi plane cut (b), and in the theta plane cut (c).

Now that the main patch has been designed, an identical patch was closely placed to this patch next to one of the radiating edges to allow for coupling. The patch with different

dimensions was placed at the other radiating edge of the patch in an effort to obtain another operating band. The dimension of one of the identical patches was kept with length of 6.94 mm and width of 9.045 mm. The other patch was arbitrarily chosen to have the same length as the spacing between the patches, 2mm, and the same width as the other patches.

The switch was simulated in the ideal state: short circuit for the “On” state and open circuit for the “Off” state. This is called by antenna designers as “hard-wire modeling”. Also, the feed point location was swept through the center of the patch to find the location where $Z_{in}=50\Omega$. The simulations from CST Microwave Studio show the following:

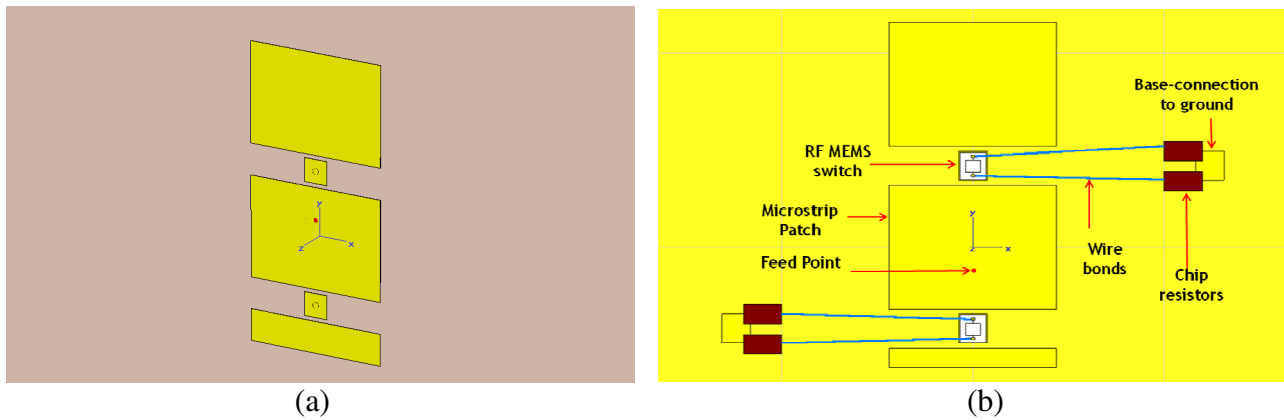


Figure 5.28 The proposed microstrip patch layout (a) without the RF MEMS switches and (b) with the switches embedded in the modeling.

Once the full layout was integrated for simulations, a change in input impedance was observed, causing a slight shift in resonant frequency. Figure 5.29 shows this effect, as the interelement spacing was also varied from 2.413-1.713mm to study its effect. The spacing was kept at $s < 0.10\lambda_0$, not representing a significant difference in coupling. The center frequency shifted to 9.75 GHz, and a decrease in bandwidth was observed.

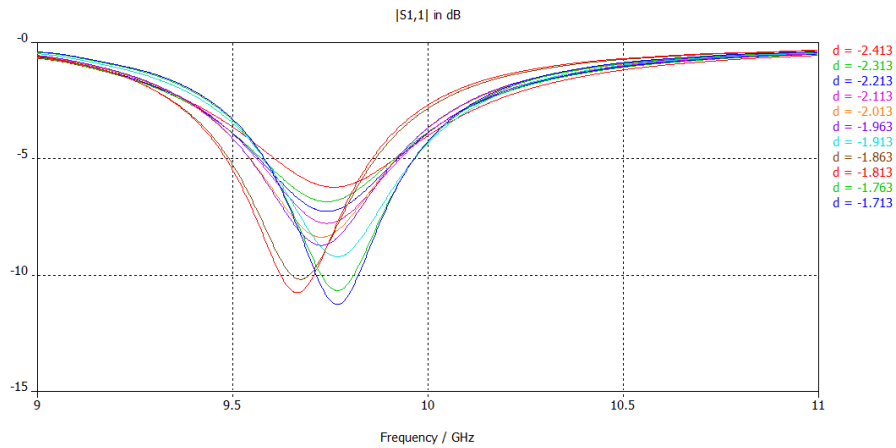


Figure 5.29 Return loss of antenna with additional patches integrated.

It can be seen that the resonant frequency shifts slightly downwards. This is due to the increasing capacitance to ground (capacitance loading) [69]. Since the results were expected, the next step was to interconnect the switches to the patches. This is the last step in the switch integration (see Figure 5.30). Once the switches were integrated the antenna was simulated again for resonance frequency. The return loss is shown in Figure 5.31, along with the VSWR (Figure 5.32), and the real impedance seen by the signal port (Figure 5.33).

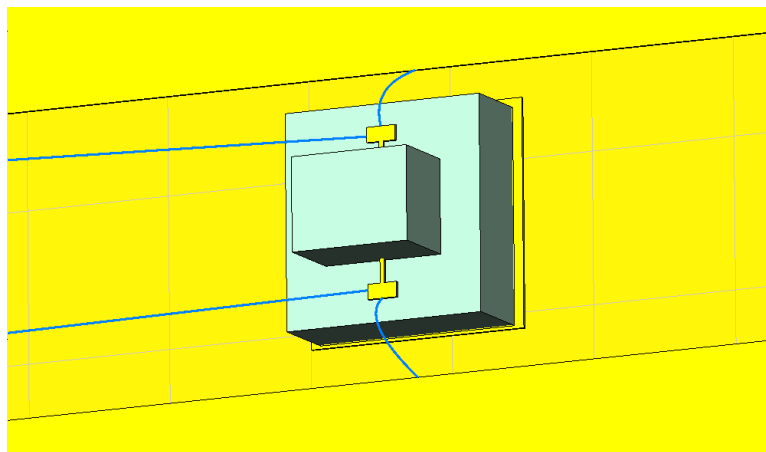


Figure 5.30 Final wiring of the switches.

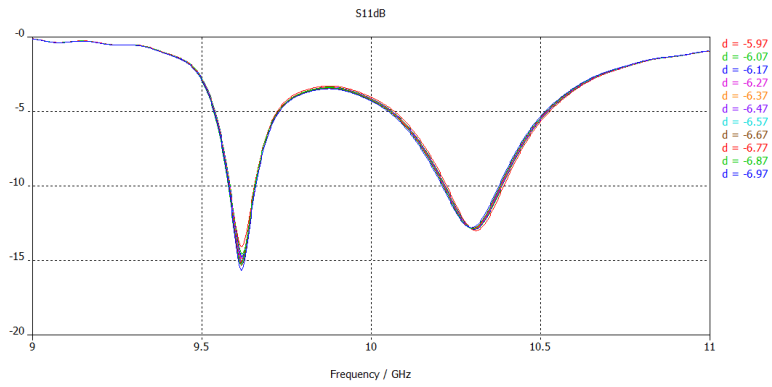


Figure 5.31 S11 for the reconfigurable microstrip patch antenna with hard wire modeling of the switches.

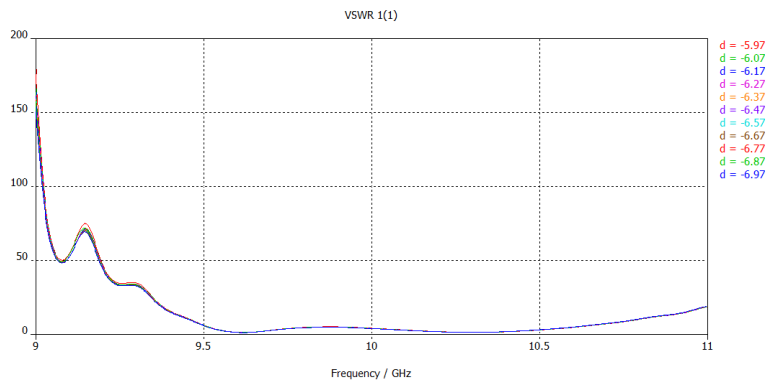


Figure 5.32 VSWR of the reconfigurable microstrip patch antenna.

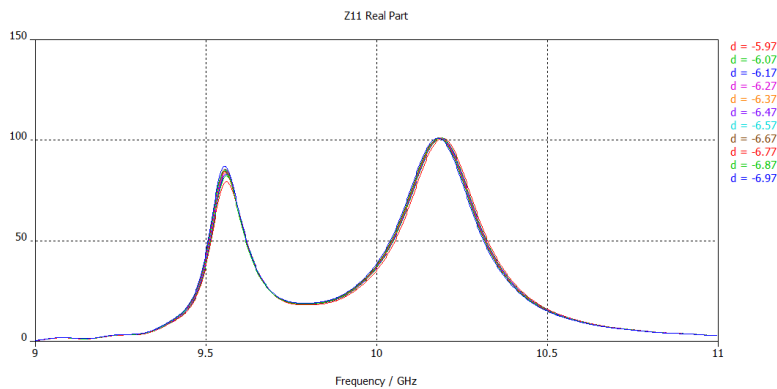


Figure 5.33 Real part of the input impedance.

The return loss and voltage standing wave ratio show the shift in resonance frequency of the antenna design after performing hard wire modeling of the RF MEMS switch. The real part of the input impedance shows that there's a good matching around two distinct operating bands. When examined from 9-11 GHz, a change was observed. The excited element was forced to couple with the surrounding patches, creating a second operating band near the same frequency. The operating frequency bands with a return loss better than a -10dB are found to be from 9.58-9.67 GHz (centered at 9.62 GHz) and 10.21-10.37 GHz (centered at 10.29 GHz). Figure 5.34 shows the same results expanding for the On-On configuration expanding the frequency under study from 2 to 18 GHz, and keeping all the design parameters to be the ones to be used during the antenna fabrication. The real part of the input impedance shows a good match at the mentioned before frequency bands.

This change in frequency demonstrates that our design indeed provides multi-frequency operation. However, the simulated case is the ideal case, where the connections were hard-wired, assuming an ideal behavior of the RF MEMS switch. The antenna was fabricated to validate these results, integrating the RF MEMS switches to electrically connect the group of printed patch radiators for operation at multiple frequencies.

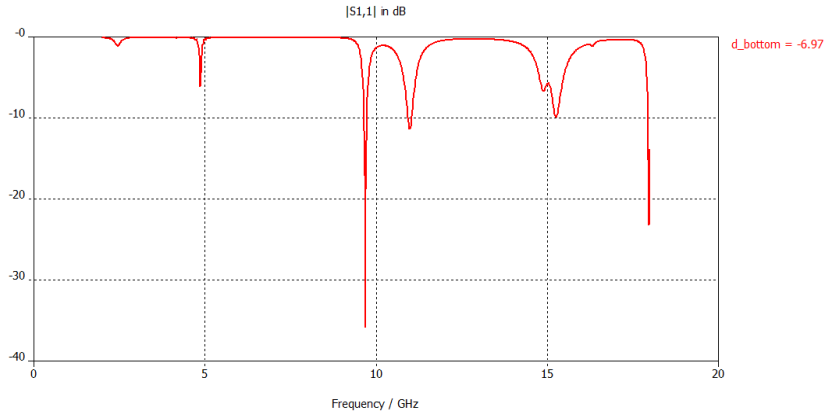


Figure 5.34. Return loss of antenna with switches in On-On state for 8-18 GHz.

5.3.4 Fabrication

The fabrication process consisted of inputting the layout in the milling machine and milling the structure (Figure 5.35(a)). There were several details to add to the layout design of the antenna to be able to integrate the switches properly. A patch is needed for the placement of the switch, a via hole for connection of this patch to the ground plane, and a patch for the integration of the protection circuit for safe static charge build-up dissipation. The via holes were connected using electroplating, thoroughly protecting the rest of the structure. Then, the connecting the probe feed in the reflow oven (Figure 5.34(b)), hand placing the RF MEMS switches (Figure 5.34(c)), and connecting the switches via wire bonding (Figure 5.34(d)).

The RF MEMS switches were integrated onto the antenna platform using wire bonding, having the wires as the RF path between the switch and the antenna. The reliability of the switches is tied to their proper handling. There are some important characteristics about them that need to be considered, such as failure mechanisms.

There are physical constraints that need to be considered. One is the size of the switch. The footprints of the switches in question are 1.37mm x 1.42mm. The milling machine has a

limitation on the path of metal it can remove from the surface layer of the substrate. The smallest drill bit is 0.250mm, which has to be taken into consideration when designing the spacing between patches.



(a) LPFK 95s/II Milling Machine



(b) GF-B Reflow Oven



(c) Placement of RMSW200 Switches



(d) KS 4123 Wire Bonder

Figure 5.35 Machinery used in the fabrication of the antennas.

The machinery used in the fabrication of the antenna required specialized training and some period of practicing, getting familiarized with the debugging procedures. The importing of the files into the milling machine controller had to be done in a specific file, named “GERBER file”. This file does not generate automatically out of the software used for simulations. They

have to be imported into another software, in this case AWR Microwave Office, in order to generate the layouts. Once the layouts were generated, they had to be exported to a new schematic within AWR. And finally, they could be exported with the proper file extension.

The designs were milled out and cleaned right after fabrication. The probe feed was then set in place after drilling the hole that will allow for the inner connector to transmit power to the antenna patch. The base for the switches had to be drilled out as well to be able to place a via and have a proper dc-ground connection with the RF MEMS switch. The switches were glued using conductive epoxy. Silver paint can also be used to achieve a positive contact between the switch and the patch. The final step was to integrate the switches to the structure via wire bonding. The wire bonding machine is a specialized tool that needs proper handling of the “Force” and “Power” settings of the machine. The slightest offset of these settings could break the wire, resulting in lots of time spent threading the needle. The experience with this machine is crucial when performing this task. Upon successful integration of all the components, then the antenna was ready for testing.

During the time of integration, there was a lot of static build up in all surfaces, causing electrostatic discharge events (ESD). ESD is a rapid transfer of electrostatic charge between two objects, usually resulting when two objects at different potentials come into direct contact with each other and it is one of the major causes of device failures in the semiconductor industry. Later versions of the switch were design to protect better against these events. ESD controls implemented were prevention of static charge build-up and safe dissipation of any charge build-up. The minimization of movements in the work area, as well as the use of ESD-safe apparel (discharge wrist bracelet) will help in minimizing static charges generated by personnel. A

protection circuit is required to provide safe dissipation of the charge build-up. The improvements in the ESD robustness of the product must be done by the manufacturer.

5.3.5 Results and Discussions

The antenna was characterized for frequency of operation. The platform used was similar to the one used in the proof of concept, a support base hold up the structure during characterization. The measurements were performed away from all reflective surfaces. It is important to mention that during the simulations the ground plane is considered to be infinite, avoiding all the diffraction caused by the wavefront impinging onto the ground plane. Figure 5.36 shows the full antenna integrated. Figure 5.37 shows the return loss measurements for the antenna before and after the actuation of both RF MEMS switches.

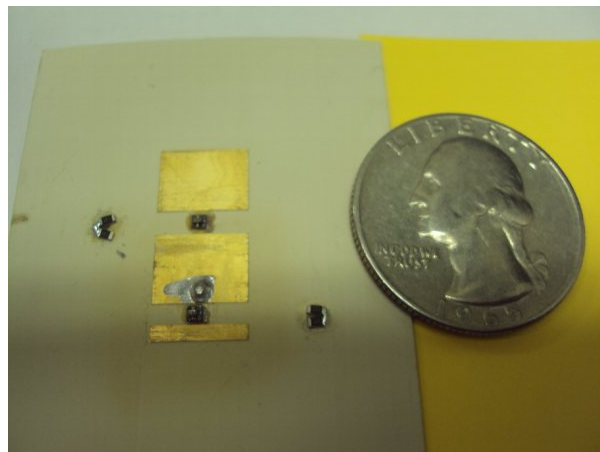


Figure 5.36 Integrated microstrip patch antenna.

The Off-Off configuration presented the first resonance of the antenna at a center frequency of 9.82 GHz in agreement with simulations. It can be observed that there is another

resonance at a higher frequency, centered at 16.3 GHz. This could be due to the coupling with the smaller patch. However, the return loss shows that it is not even at -6 dB. A substantial change should be seen when the switches get actuated.

The resonance frequency is shown to change the resonance frequency of the patch upon actuation of the RF MEMS switches. The results also show an excitation at a higher frequency not observed in the simulations. It was expected that the resonance frequency would stay in the vicinity of the design of the main patch, and decreasing from 10 GHz. Therefore, the simulations were limited to 11 GHz.

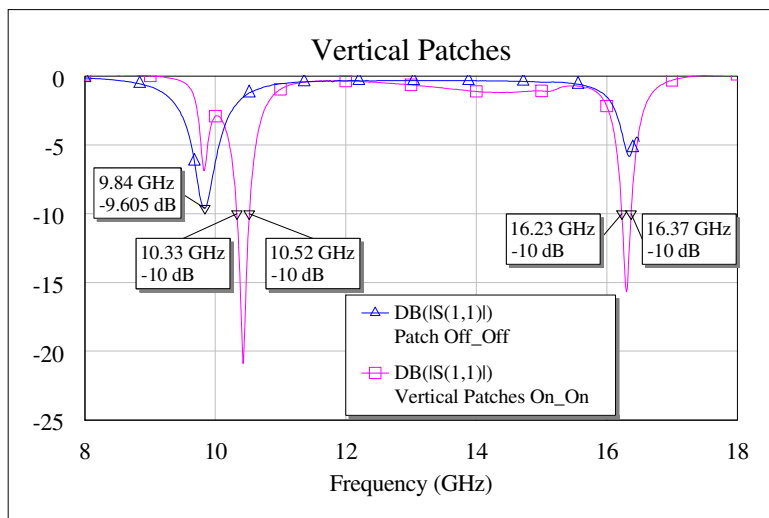


Figure 5.37 Return loss as a function of frequency of the reconfigurable microstrip patch with actuation of the switches.

The simulation for the reconfigurable microstrip patch antenna was repeated, expanding the frequency range in order to compare against measured data. Figure 5.31 was focused in the 9 GHz to 11 GHz frequency range. The simulations showed that there's a higher order mode being excited, which was validated with the antenna measurements. Figure 5.36 shows the results.

5.4 Additional Reconfigurable Antenna Designs

The next design was simulated using the same technique of hard wire modeling as the microstrip antenna. It showed that it is a very desirable design to work on with promising development for frequency and radiation pattern reconfiguration.

5.4.1 Spiral Antenna

The spiral antenna has three configurations even though the switch states are a two bit configuration (four possible combinations). The reason is that the actuation of the second switch doesn't provide a conductive path for the current distribution, due to the isolation of the first switch. The first configuration is the "Off-Off" which will be called the "monopole configuration" of the antenna. Once the first switch is actuated, the antenna turns into a $\frac{3}{4}$ of a spiral, increasing the electrical length by a factor of 3. The last configuration is a full square spiral antenna with a total width that is the same as the size of the monopole.

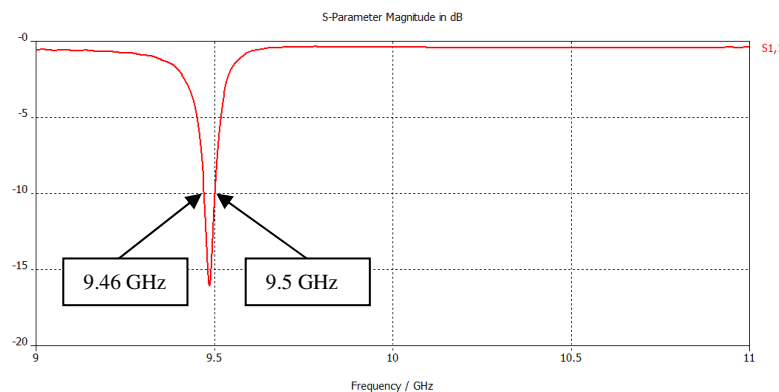
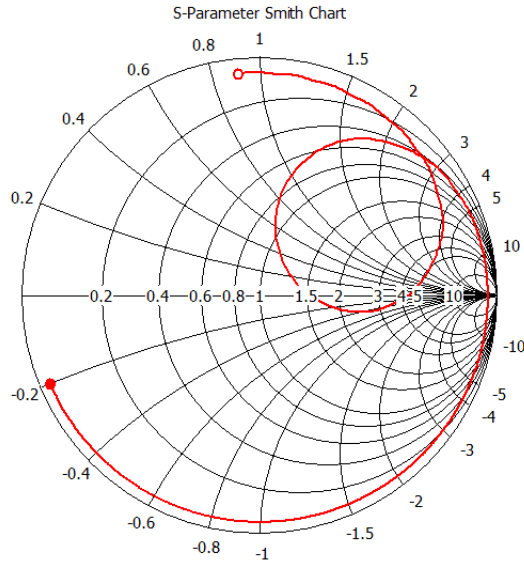


Figure 5.38 Return loss as a function of frequency of the reconfigurable spiral antenna in the monopole configuration.

- 9.000 (2.939, 45.16) Ohm
- 11.00 (1.107, -10.11) Ohm

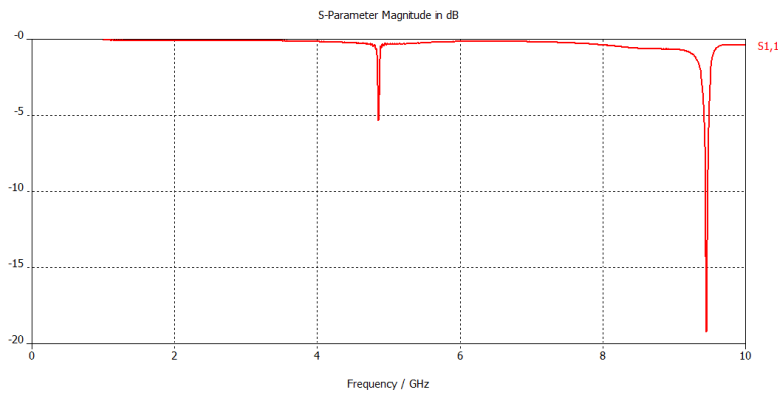
S1,1 (50 Ohm)



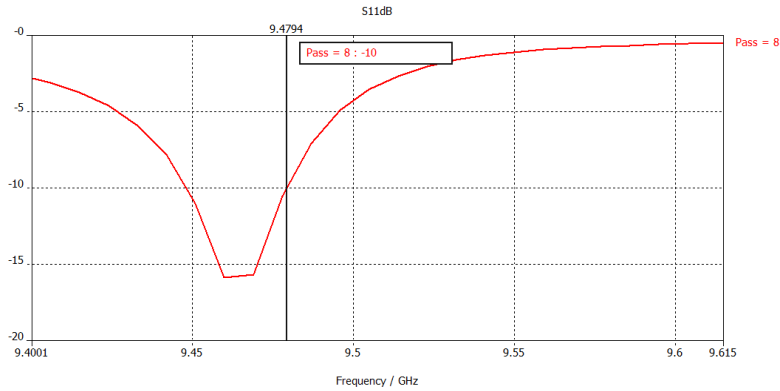
Parameter = Frequency / GHz

Figure 5.39 Return loss as a function of frequency of the reconfigurable spiral antenna in the monopole configuration plotted in Smith Chart.

By actuating the first switch the antenna changes from the monopole configuration to the first spiral configuration, providing a different path for current.



(a)



(b)

Figure 5.40 Return loss of spiral configuration as a function of frequency.

The resonance frequency stayed fairly in the same range as in the monopole configuration, which was from 9.46 GHz to 9.5 GHz. For the spiral configuration, the resonance frequency ranges from 9.44 GHz to 9.48 GHz. It shows barely a change in frequency, but it is expected to change radiation pattern. Careful design might lead to simply a reconfigurable radiation pattern antenna.

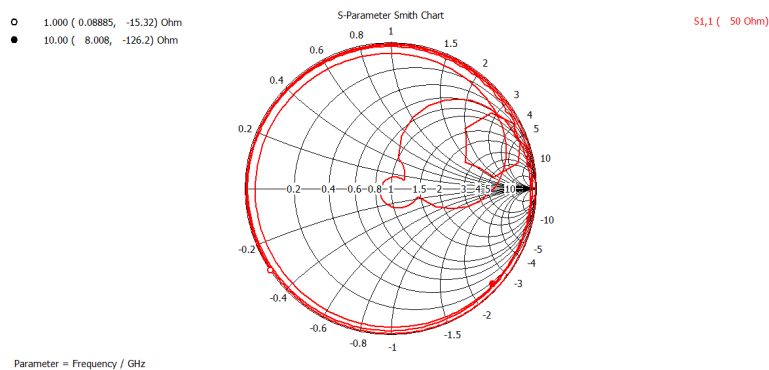


Figure 5.41 Return loss as a function of frequency of the reconfigurable spiral antenna with one switch simulated in “On” state plotted in Smith Chart.

Since there was no change in resonant frequency, as expected, the radiation patterns must be studied to determine the pattern reconfigurability of the antenna.

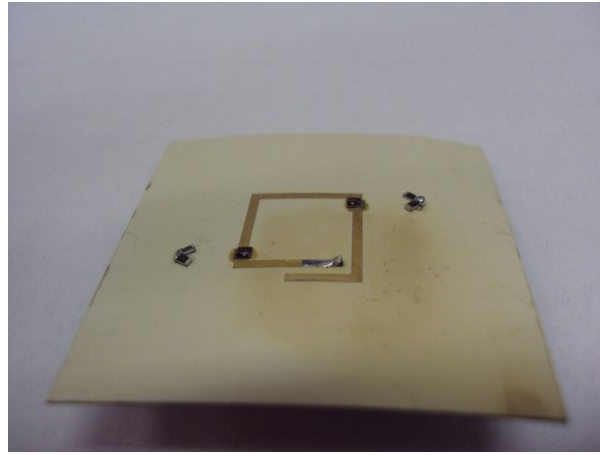


Figure 5.42 Integrated monopole-spiral antenna.

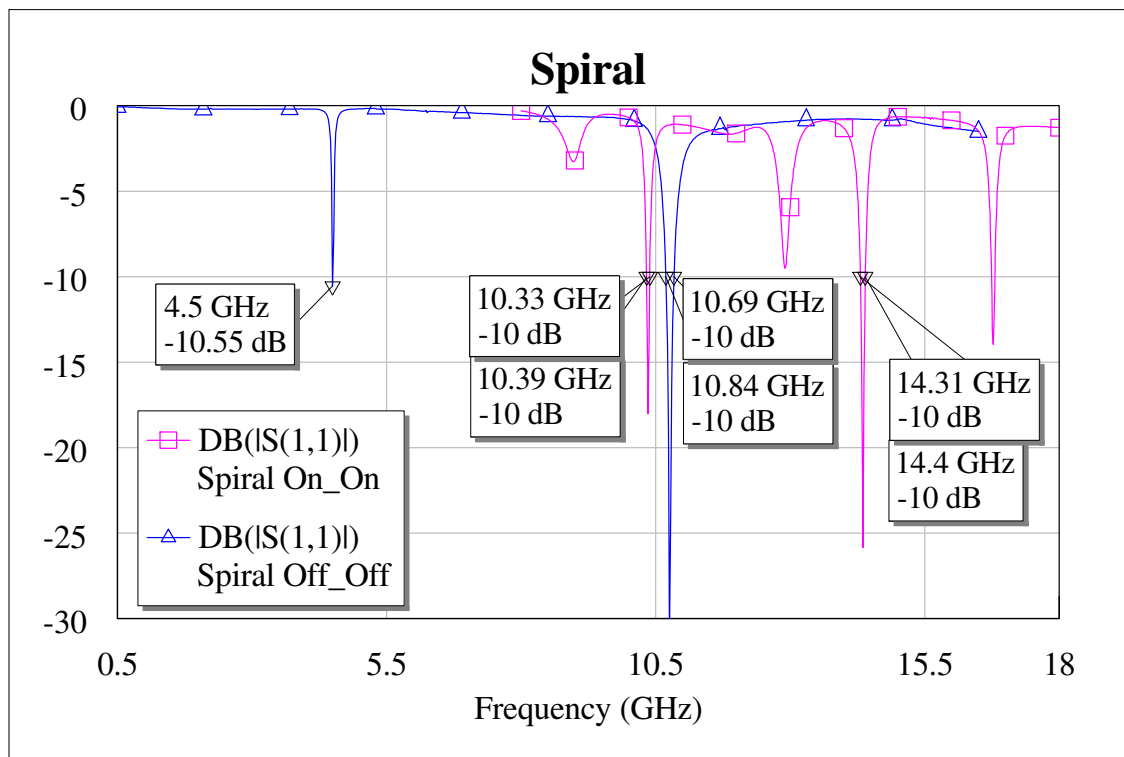


Figure 5.43 Return loss of the monopole-spiral antenna.

The measurements are in agreement with simulations. There is a shift in resonant frequency from simulations in the Off-Off configuration from 9.5 GHz to 10.36 GHz center frequency. The On-On configuration also stayed in the 9.44 GHz to 9.48 GHz during simulations, but also presents a shift in frequency when measured. The measured resonant frequency channel goes from 10.69 GHz to 10.64 GHz. The reconfiguration of the resonant frequency is shown, but fine tuning of the connection of the probe feed might help with keeping the same resonant frequency. The radiation patterns have to be studied to prove pattern reconfigurability.

Chapter 6

Conclusions and Recommendations

6.1 Conclusions

- **Matching of the system**

The challenge for the antenna engineer is optimizing the antenna efficiency and matching the antenna to the source or load over the desired bandwidth. It seems that a different feeding technique (microstrip line) may be more suitable for integrating a matching network, i. e. tuning stubs, even though the feed produces spurious radiation. An inset feed must be implemented.

- **Proof of concept**

The proof of concept supported the hypothesis that lumped off-the-shelf RF MEMS switches could be integrated into an antenna structure and used to tune the antenna in order to have multiple resonances. A control system is needed to actuate the switches independently.

- **RF MEMS switch characterization**

The Radant MEMS switches used in the fabrication of the different antenna structures performed somewhat similar to what the manufacturer advertised. The variations in performance could be due to the age of the switches and the inexperience handling these types of devices. New techniques must be developed in order to ease their assembly for control purposes. Also, the use of wire bonding should be eliminated since it inputs a variable that cannot be controlled: the length of the wires. Future testing needs to be done in order to understand their effects on the antennas operating at the X-band.

- **Actuation of the RF MEMS switches**

A control system may ease the characterization of the antenna structures employing RF MEMS switches. This will avoid actuation of the switches by hot switching, which causes failure if short circuited and shortens the life of the switch. An FPGA platform might be suitable for this task. This could lead to beam steering capabilities.

- **Biasing lines**

The biasing lines were implemented using wire bonding. This method provides no controlled in the length of the wires used. The only way to minimize their effect is by establishing pre-milled dc-bias lines to a point where they do not cause interference or coupling with the resonating structure.

- **Microstrip patch antenna**

The most important achievement of this thesis research was the design and characterization of the RF MEMS-based reconfigurable microstrip patch antenna. The tunability of the frequency was achieved. The variation of the location of the probe feed was simulated to result in the best matching possible with probe feeding technique. This feeding technique doesn't allow implementing a matching network, increasing the time required to attain the best results possible after integration. A microstrip feed with a matching network might be considered, even though it provides spurious radiation. The changing in the coupling between closely spaced patches was changed with the integration of the RF MEMS switches. Some other geometries and configurations can be achieved with this type of technology as well.

The resonance frequency was analyzed to determine the antenna's tuning capability. Another extension to the main patch was added to the design in order to keep the feed point at the place where it is expected to have an input impedance of 50Ω . The goal response of the

operating frequency at the X-band was achieved with low return loss, proving the reconfiguration capability of the antenna.

The following objectives were met after finishing the thesis:

- Designed an RF-MEMS based reconfigurable antenna with off-the-shelf components for proof of concept.
- Showed the advantage of MEMS switches regarding linearity and insertion loss.
- Characterized the MEMS switches to be used with the reconfigurable antennas.
- Simulated and validated the hypothesis of designing an antenna design with reconfigurable behavior.

Two issues remain attached to the RF MEMS switches that one should consider. The sensitivity to electrostatic discharge and hot switching, due to high bias voltage or thermal effects, which can permanently damage the switch, and their power handling capabilities limited by the self actuation and stiction in the down state due to high incident RF power. The power handled by the RF MEMS switches is low and can be mostly considered for low power applications, ranging from the 10's of mW for ohmic switches and up to 1W for capacitive switches [70].

The progress on the tasks established in the objective was reported herein, to include approach, process, problems, solutions, and resulting performance of the antenna system fabricated. The change in coupling between the main driven element and the parasitic structures to alter the frequency of operation of the antenna was achieved. The results and progress were compiled into two research paper submitted for publication.

6.2 Recommendations

RF MEMS have proven to be effective in achieving an antenna reconfiguration. This approach should be used in the fabrication of new antennas that can be implemented in the new communications systems with constantly changing requirements. They can assist in the continuous search for improvement in power handling and reliability so that the increasing demand to operate in network systems with different standards and operating frequencies can be met.

For future designs, there are several things that can be changed. The simulations can be more specific in predicting the antenna behavior if the interconnection between the probe feed and the patch is analyzed in more details, to include the integration of a circuit model for the switch into the structure to be analyzed. This was the intent of characterizing the RF MEMS switch, but could not be integrated into the simulations with the electromagnetic codes available. A more careful and detailed analysis of the trade-offs could also be done to get a bigger bandwidth or a better return loss. Nevertheless, the hard wire modeling proved to be accurate.

References

1. Amanda M. Castro, "Tunable Folded-Slot Antenna with Thin Film Ferroelectric Material", Master of Science Thesis, University of Puerto Rico, Mayagüez, 2003.
2. Microwave Encyclopedia, "Microstrip Patch Antennas", January 5, 2008.
3. G. A. Deschamps, "Microstrip microwave antennas", *3rd United States Air Force Symposium on Antennas*, 1953.
4. D. H. Schaubert, D. M. Pozar, A. Adrian, "Effect of Microstrip Antenna Substrate Thickness and Permittivity: Comparison of Theories with Experiment", *IEEE Transactions on Antennas and Propagation*, Vol. 37, No. 6, June 1989, pp. 677-682.
5. Y. T. Lo, W. F. Richards, J. E. Brewer (University of Illinois at Urbana Champaign), "Evaluation of Losses in Microstrip Antenna Materials", *Defense Technical Information Center*, April 1980.
6. L. Brillouin, "Wave Propagation And Group Velocity", Academic Press Inc., New York and London, 1960.
7. I. J. Bahl, D. K. Trivedi, "A Designer's Guide to Microstrip Line", *MicroWaves*, May 1977, pp.174-182.
8. F. Mohammed Ali, Al-Raie (The Polytechnic Higher Institute of Yefren, Libya), "Estimated Microstrip Substrate Relative Dielectric Constant", *Microwaves and RF*, December 2007.
9. A. H. Taqi, R. A. Al-Rashid, A. M. Jassim, "An Experimental Investigation of a Short Backfire Antenna with Electromagnetic Coupled Patch as Feed Element", *Journal of Islamic Academy of Sciences* 8:2, 61-68, 1995.
10. C. A. Balanis, "Antenna: Theory, Analysis and Design", 2nd Edition, John Wiley & Sons, Inc., 1997.

11. Y. T. Lo, C. E. Skupien, S. S. Zhong, "A Study of Microstrip Antennas for Multiple Band Operation", *Defense Technical Information Center*, Final technical report, Sept 82.
12. A. H. M. Zahirul, Alam, N. B. Mohd Sahar, N. B. Zamani, "Design of MEMS Based Triple Band Reconfigurable Antenna", *4th International Conference on Information and Communications Technology*, December 2006.
13. R. Garg, P. Bhartia, I. Bahl, A. Ittipiboon, "Microstrip Antenna Design Handbook", 2000.
14. Rogers Corporation, "Width and Effective Dielectric Constant Data for Design of Microstrip Transmission Lines on Various Thicknesses, Types and Claddings of TMM® Microwave Laminates", *High Frequency Circuit Materials*, 1999, TM 3.3.3.
15. F. Mohammed Ali, Al-Raie (The Polytechnic Higher Institute of Yefren, Libya), "Estimated Microstrip Substrate Relative Dielectric Constant", *Microwaves and RF*, December 2007.
16. D. Guha (University of Calcutta, India), "Broadband design of microstrip antennas: Recent trends and developments", *Mechanics, Automatic Control and Robotics*, Vol. 3, No. 15, 2003, pp. 1083 – 1088.
17. J. Grzyb, G. Tröster, "MM-Wave Microstrip Patch and Slot Antennas on Low Cost Large Area Panel MCM-D Substrates – A Feasibility and Performance Study", *IEEE Transactions on Advanced Packaging*, Vol. 25, No. 3, August 2002, pp. 397-408.
18. R. A. York (University of California in Santa Barbara), "Review of Transmission Line Theory", Course ECE 134.
19. K. R. Carver (New Mexico State University), J. W. Mink (U. S. Army Research Office), "Microstrip Antenna Technology", *IEEE Transactions on Antennas and Propagation*, Vol. AP-29, No. 1, January 1981.

20. Electrical Engineering Training Series, Integrated Publishing , NEETS Module 10, "Introduction to Wave Propagation, Transmission Lines, and Antennas" www.tpub.com
21. Griffiths, David. "Chapter 9: Electromagnetic Waves", in Alison Reeves (ed.): *Introduction to Electrodynamics*, 3rd edition, Upper Saddle River, New Jersey, Prentice Hall, 394. ISBN 0-13-805326-x. OCLC 40251748
22. Ramo, Whinnery, Van Duzer, *Fields and Waves in Communications Electronics*, John Wiley and Sons, 1994.
23. D. M. Pozar, Microstrip Antenna, *Proceedings of the IEEE*, Vol. 80, No. 1, January 1992.
24. IEEE Standard Definitions of Terms for Antennas (IEEE Std 145-1983).
25. M. J. Vaughan, K. Y. Hur, R. C. Compton, "Improvement of Microstrip Patch Antenna Radiation Patterns", *IEEE Transactions on Antenna Propagation*, Vol. 42, No. 6, June 1994.
26. D. M. Pozar, D. Schaubert, *Microstrip Antennas: The Analysis and Design of Microstrip Antennas and Arrays*, page 57, 1995.
27. D. Pozar, "Five novel feeding techniques for microstrip antennas", *Antennas and Propagation Symposium*, Vol. 25, pp. 920-923, 1987.
28. B. M. Alarjani, J. S. Dahele, "Feed reactance of rectangular microstrip patch antenna with probe feed", *Electronics Letters*, Vol. 36, Issue 5, pp. 388-390, March 2000.
29. F. Islam, M.A. Mohd, B.Y. Majlis, "Design and Simulation of X-Band Micromachined Microstrip Antenna", *5th Student Conference on Research and Development SCORED-2007*, Malaysia, Decmber 11-12, 2007.
30. L. I. Basilio, M. A. Khayat, *et. al.*, "The Dependence of the Input Impedance on Feed Position of Probe and Microstrip Line-Fed Patch Antennas", *IEEE Transactions on Antennas and Propagation*, Vol. 49, No. 1, January 2001.

31. D. H. Schaubert, D. M. Pozar, A. Adrian, "Effect of Microstrip Antenna Substrate Thickness and Permittivity: Comparison of Theories with Experiment", *IEEE Transactions on Antennas and Propagation*, Vol. 37, No. 6, June 1989.
32. P. S. Nakar, "Chapter 3: Microstrip Patch Antenna", Florida State University Thesis, Electrical Engineering Department.
33. K. Li, C. H. Cheng, *et. al.*, "Coplanar patch antennas: principle, simulation and experiment", *IEEE Antennas and Propagation Symposium 2001*, Vol. 3, pp. 402-405, July 2001.
34. J. T. Bernhard (University of Illinois at Urbana Champaign), "Reconfigurable Antennas", Morgan & Claypool Publisher, pp. 5, 2007.
35. C. A. Balanis, "Antenna: Theory, Analysis and Design", 3rd Edition, John Wiley & Sons, Inc., 2005.
36. J. T. Bernhard, "Compact single-arm square spiral microstrip antenna with tuning arms," *IEEE AP-International Symposium Digest*, Vol. 2, pp. 696-699, July, 2001.
37. A. T. Kolsrud, M.-Y. Li, and K. Chang, "Dual-frequency electronically tunable CPW-fed CPS dipole antenna," *Electronics Letters*, vol. 34, pp. 609-611, 1998.
38. C. Luxey, L. Dussopt, J.-L. Le Sonn, and J.-M. Laheurte, "Dual-frequency operation of CPW-fed antenna controlled by *pin* diodes", *Electron Letters.*, Vol. 36, pp. 2-3, 2000.
39. C. Panagamuwa, A. Chauraya, J. Vardaxoglou, "Frequency and Beam Reconfigurable Antenna Using Photoconducting Switches", *IEEE Transactions on Antennas and Propagation*, Vol. 54, No. 2, pp. 449-454, February 2006.
40. D. E. Anagnostou, G. Zheng, L. Feldner, M. T. Chryssomallis, J. C. Lyke, J. Papapolymerou, and C. G. Christodoulou, (Georgia Institute of Technology, GA), "Silicon-etched re-

- configurable self-similar antenna with RF-MEMS switches,” in *Proc. Antennas and Propagation Society Symposium*, vol. 2, pp. 1804–1807, Jun. 20–25, 2004.
41. C. Puente-Baliarda, J. Romeu, R. Pous, and A. Cardama (Polytechnic University of Catalonia, Barcelona, Spain), “On the behavior of the Sierpinski multiband fractal antenna,” *IEEE Transactions on Antennas and Propagation*, vol. 46, no. 4, pp. 517–524, Apr. 1998.
42. D. E. Anagnostou, *et al.*, “Design, fabrication, and measurements of an RF-MEMS-Based self similar reconfigurable antenna”, *IEEE Transactions on Antennas and Propagation*, Vol. 54, No. 2, February 2006.
43. G. M. Rebeiz, “RF MEMS: Theory, Design, and Technology”, Chapter 13, N.J. 2003.
44. G. H. Huff, J. Feng, S. Zhang, J. T. Bernhard, “A Novel Radiation Pattern and Frequency Reconfigurable Single Turn Square Spiral Microstrip Antenna”, *IEEE Microwave and Wireless Components Letters*, Vol. 13, No. 2, pp. 57-59, February 2003.
45. J. A. Zamrni, A. Muscat, “A small tunable antenna using multiple shorting posts and varactor diodes”, *2008 International Symposium on Communications, Control and Signal Processing*, pp. 83-86, March 2008.
46. E. R. Brown, “RF-MEMS switches for reconfigurable integrated circuits,” *IEEE Transactions on Microwave Theory and Techniques*, vol. 46, no. 11, pp. 1868–1880, Nov. 1998.
47. A. S. Daryoush, K. Bontzos, P.R. Hercsfeld (Drexel University, Philadelphia, PA), “Optically tuned patch antenna for phased array applications”, *IEEE Antennas and Propagation International Symposium*, pp. 361–364.

48. G. Rebeiz, W. H. Weedon, W. J. Payne, "MEMS-Switched Reconfigurable Antennas", *IEEE Antennas and Propagation Society International Symposium*, Boston, MA, Volume: 3, pp. 654-657, July 8-13, 2001.
49. D. E. Anagnostou, G. Zheng, L. Feldner, M. T. Chryssomallis, J. C. Lyke, J. Papapolymerou, and C. G. Christodoulou (Georgia Institute of Technology, GA), "Silicon-etched reconfigurable self-similar antenna with RF-MEMS switches," in *Proc. Antennas and Propagation Society Symposium*, vol. 2, pp. 1804–1807, Jun. 20–25, 2004.
50. G. H. Huff, J. T. Bernhard (University of Illinois at Urbana-Champaign, IL), "Integration of Packaged RF MEMS Switches With Radiation Pattern Reconfigurable Square Spiral Microstrip Antennas", *IEEE Transactions on Antennas and Propagation*, Vol. 54, No. 2, February 2006.
51. Chang won Jung, Ming-jeer Lee, G. P. Li, and Franco De Flaviis (University of California at Irvine, CA), "Reconfigurable Scan-Beam Single-Arm Spiral Antenna Integrated With RF-MEMS Switches", *IEEE Transactions on Antennas and Propagation*, Vol.54, No. 2, pp. 455-463, February 2006.
52. R. Jackson Jr., R. Ramadoss (Auburn University, AL), "A MEMS-based electrostatically tunable circular microstrip patch antenna", *Journal of Micromechanics and Microengineering*, 2007, Vol. 17, pp. 1-8.
53. R. Jackson, *et al.*, "MEMS based electrostatically tunable microstrip patch antenna fabricated using printed circuit processing techniques", *IEEE Antennas Wireless Propagation Letters*, pp. 228-30, 2006.
54. S. Majumder, J. Lampen, R. Morrison, J. Maciel, "MEMS Switches", *IEEE Instrumentation & Measurement Magazine*, March 2003.

55. Y. E. Erdemli, R. A. Gilbert, J. L. Volakis (Ohio State University), "A Reconfigurable Slot Aperture Design Over a Broad-Band Substrate/Feed Structure", *IEEE Transactions on Antennas and Propagation*, Vol. 52, No. 11, November 2004, pp. 2860-2870.
56. J. H. Schaffner, D. F. Sievenpiper, R. Y. Loo (HRL Laboratories, Malibu, CA), J. J. Lee, S. W. Livingston (Raytheon, El Segundo, CA), "A Wideband Beam Switching Antenna Using RF MEMS Switches", special session *SS-3 MEMS For Antenna Applications*, *IEEE Antennas and Propagation Society International Symposium 2001*, Vol. 3, pp. 658-661.
57. J. H. Schaffner, *et. al.*, "Reconfigurable Aperture Antennas Using RF MEMS Switches for Multi-Octave Tunability and Beam Steering", *Proceedings 2000 IEEE Antennas and Propagation Symposium*, Salt Lake City, pp. 321-324.
58. Chang won Jung, *et al.*, "RF-MEMS Capacitive Series Switches of CPW & MSL Configurations for Reconfigurable Antenna Application", *EMC Europe Workshop 2005*, Rome, Italy.
59. Wang, B. Z., Xiao, S., and Wang, J., "Reconfigurable patch-antenna design for wideband wireless communication systems," *IET Microwaves, Antennas & Propagation*, Vol. 1, No. 2, pp. 414-419, April 2007.
60. Kraus, J.D., and Marhefka, R.J., *Antennas for All Applications*, 3rd ed., McGraw-Hill, New York, 2002.
61. D. J. Roscoe, L. Shafai, A. Ittipiboon, M. Cuhaci, R. Douville, "Tunable dipole antennas," *Proceedings of the IEEE/URSI International Symposium on Antennas and Propagation*, Vol. 2, pp. 672-675, 1993.
62. Radant MEMS, 255 Hudson Road, Stow, MA 01775.

63. Filipovic, D.S., and Volakis, J.L., "A flush-mounted multifunctional slot aperture (comboantenna) for automotive applications," *IEEE Transactions on Antennas and Propagation*, Vol. 52, pp. 563-571, February 2004.
64. G. M. Rebeiz, "RF MEMS: Theory, Design, and Technology", Chapter 13, N.J. 2003.
65. Radant MEMS, "Application Note for Test and Handling of SPST RF MEMS", www.radantmems.com, 2005.
66. E. J. Denlinger, "Radiation from Microstrip Radiators", *IEEE Transactions on Microwave Theory and Techniques*, Vol. 17, No. 4, pp.235-236, April 1969.
67. D. M. Pozar, "Input Impedance and Mutual Coupling of Rectangular Microstrip Antennas", *IEEE Transactions on Antennas and Propagation*, Vol. AP-30, No. 6, pp. 1191-1196, November 1982.
68. R. P. Jedlicka, M. P. Toe and K. R. Carver, "Measured mutual coupling between microstrip antennas" *IEEE Transactions on Antennas and Propagation*, Vol. A-P 29, pp. 147-149, January 1981.
69. Steve Best, "Electrically Small Antennas Webinar", presented on October 20, 2009, sponsored by CST of America and Microwave Journal, <http://event.on24.com/r.htm?e=169384&s=1&k=56C8FEF37E6AAF1FC0B63D75B3136196>
70. J. Park, "Fabrication and measurements of direct contact type RF MEMS switch", *IEICE Electronics Express*, Vol. 4, No. 10, pp. 319-325, 2007.